

**Jagiellonian University in Cracow**  
Faculty of Physics, Astronomy and Applied Computer Science

**Daria Kamińska**  
Student number: 1055739

**Measurement of the charge asymmetry for the**  
 **$K_S \rightarrow \pi e \nu$  decay with the KLOE detector**

Master thesis  
Major: Experimental Physics  
Specialisation: Nuclear Physics

Supervised by  
prof. dr hab. Paweł Moskał  
Institute of Physics  
Division of Nuclear Physics  
and  
dr Eryk Czerwiński  
Institute of Physics  
Division of Nuclear Physics

Cracow, 2014

**Oświadczenie autora pracy**

Świadom odpowiedzialności prawnej oświadczam, że niniejsza praca dyplomowa została napisana przeze mnie samodzielnie i nie zawiera treści uzyskanych w sposób niezgodny z obowiązującymi przepisami.

Oświadczam również, że przedstawiona praca nie była wcześniej przedmiotem procedur związanych z uzyskaniem tytułu zawodowego w wyższej uczelni.

Kraków, dnia

Podpis autora pracy

**Oświadczenie kierującego pracą**

Potwierdzam, że niniejsza praca została przygotowana pod moim kierunkiem i kwalifikuje się do przedstawienia jej w postępowaniu o nadanie tytułu zawodowego.

Kraków, dnia

Podpis kierującego pracą

# *Abstract*

The aim of this work is a determination of the charge asymmetry in semileptonic decays of  $K_S$  meson. The measurement was performed using KLOE detector localized at DAΦNE accelerator in the National Laboratory in Frascati, Italy. The experimental data used in this thesis has been collected during 2004-2005 data campaign of KLOE. The final values of charge asymmetry determined for  $K_S$  meson semileptonic decays, obtained by registering the  $\phi \rightarrow K_L K_S \rightarrow K_L \pi^\mp e^\pm \nu(\bar{\nu})$  process, amount to  $A_S = (1.5 \pm 5.8_{stat}) \cdot 10^{-3}$ . Obtained result does not indicate the  $\mathcal{CP}\mathcal{T}$  violation and received statistical uncertainty is, as expected, about two times better with respect to previous measurement.



# *Streszczenie*

Celem tej pracy jest wyznaczenie asymetrii ładunkowej dla semileptonowych rozpadów mezonu  $K_S$ . Pomiary były przeprowadzone za pomocą detektora KLOE zlokalizowanego na akceleratorze DAΦNE w Narodowym Centrum Fizyki Nuklearnej we Frascati we Włoszech. Praca została napisana w oparciu o dane zebrane w latach 2004-2005. W wyniku przeprowadzonej analizy, w oparciu o liczbę zrekonstruowanych zdarzeń odpowiadających procesom  $\phi \rightarrow K_L K_S \rightarrow K_L \pi^\mp e^\pm \nu(\bar{\nu})$ , wyznaczono następującą wartość asymetrii ładunkowej:  $A_S = (1.5 \pm 5.8_{stat}) \cdot 10^{-3}$ . Otrzymany wynik nie wskazuje na łamanie symetrii  $\mathcal{CPT}$  oraz charakteryzuje się około dwukrotnie mniejszą niepewnością statystyczną niż najdokładniejszy wynik uzyskany w dotychczasowych eksperymentach.



# Contents

<b>Abstract</b>	<b>i</b>
<b>Streszczenie</b>	<b>iii</b>
<b>1 Introduction</b>	<b>1</b>
<b>2 Neutral kaon physics</b>	<b>3</b>
2.1 Neutral kaon states . . . . .	3
2.2 CP violation . . . . .	4
2.3 Charge asymmetry in semileptonic decays of $K_S$ meson . . . . .	5
2.3.1 Experimental verification . . . . .	8
<b>3 KLOE experiment at DAΦNE</b>	<b>11</b>
3.1 DAΦNE collider . . . . .	11
3.2 KLOE detector . . . . .	13
3.2.1 The drift chamber . . . . .	14
3.2.2 The calorimeter . . . . .	15
<b>4 Registration of the <math>\phi \rightarrow K_L K_S \rightarrow K_L e^\pm \pi^\mp \nu</math> process at KLOE</b>	<b>19</b>
4.1 $K_L$ measurement - $K_S$ tagging . . . . .	19
4.2 $K_S$ identification . . . . .	22
4.2.1 $K_S \rightarrow \pi e \nu$ events preselection . . . . .	22
4.2.2 Particle identification with Time of Flight method . . . . .	24
<b>5 Measurement of charge asymmetry for <math>K_S \rightarrow \pi^\mp e^\pm \nu(\bar{\nu})</math> decay</b>	<b>29</b>
5.1 Normalization procedure . . . . .	29
5.2 Estimation of the number of $K_S \rightarrow \pi^\mp e^\pm \nu(\bar{\nu})$ events . . . . .	35
5.3 Charge asymmetry . . . . .	36
<b>6 Conclusions</b>	<b>37</b>
<b>Acknowledgements</b>	<b>39</b>
<b>Bibliography</b>	<b>40</b>



# Chapter 1

## Introduction

Relation between symmetries and conservation laws was formulated in 1918 by Amalie Emmy Noether and nowadays it is referred to as Noether's theorem and it states, that for every global continuous symmetry exists an associated time independent quantity [1]. Thus the invariance of laws of physics under translations of time, space or rotation implies conservation of energy, momentum, or angular momentum, respectively. The discrete symmetries of nature such as charge conjugation ( $\mathcal{C}$ ), parity ( $\mathcal{P}$ ) or time reversal ( $\mathcal{T}$ ) do not lead to new conserved quantities. Nevertheless, all of mentioned symmetries plays an important role in particle physics, especially in calculations of the cross sections and decay rates.

Weak interaction does not conserve the  $\mathcal{C}$ ,  $\mathcal{P}$ ,  $\mathcal{T}$  or combined  $\mathcal{CP}$  symmetry. In the Standard Model the  $\mathcal{CP}$  violation is included by introducing the Cabibbo-Kobayashi-Maskawa (CKM) [2] or Pontecorvo-Maki-Nakagawa-Sakata (PMNS) [3] matrices describing mixing in quark or neutrino sector, respectively. Up to now, there is no indication of  $\mathcal{CPT}$  symmetry violation [4], which would also imply the break of Lorentz symmetry [5]. A special role in  $\mathcal{CPT}$  violation searches plays a neutral kaon system which, due to a sensitivity to a variety of symmetry violation effects, is one of the best candidates for such kind of studies. One of the possible tests is based on comparison between semileptonic asymmetry in  $K_S$  decays ( $A_S$ ) and the analogous asymmetry in  $K_L$  decays ( $A_L$ ) [6]. So far the  $A_L$  [7] was determined with a precision more than two orders of magnitude better than  $A_S$  [8]. The present accuracy of  $A_S$  determination is dominated by the statistical uncertainty. Therefore the main aim of this work is a determination of  $A_S$  with two times smaller statistical error due to four times bigger data sample.

This thesis presents determination of the  $K_S \rightarrow \pi^\mp e^\pm \nu(\bar{\nu})$  charge asymmetry based on the data sample gathered in 2004-2005 with the KLOE detector situated at DAΦNE, the Frascati  $\phi$  factory. DAΦNE is a  $e^+e^-$  collider designed to work at the energy corresponding to the  $\phi$  meson mass with high luminosity providing conditions for most complete and precise set of measurements in kaon physics and other studies

such as  $\eta, \eta'$  decays [9, 10] and searches for dark forces [11]. The  $\phi$  decay products are registered using the KLOE detector setup which is a barrel-shaped detector. Due to pair production of kaons and therefore so called tagging procedure, their rare decays (such as  $K_S \rightarrow \pi e \nu$  and  $K_S \rightarrow e \pi \nu$ ) can be identified with great precision.

The work is divided into six chapters. In the next chapter a brief theoretical introduction on phenomenology of semileptonic decays of neutral kaon is given. Third chapter contains a description of the KLOE apparatus. The characteristics and the performance of the main sub-detectors (drift chamber and electromagnetic calorimeter) are reported. The fourth chapter is devoted to description of data analysis. A  $K_S$  tagging algorithm, based on the identification of cluster produced by  $K_L$  interaction in the calorimeter, and criteria used to select a  $K_S \rightarrow \pi e \nu$  decays are presented. Obtained results are shown in chapter five, leading to the conclusions and further plans summarized in the last chapter.

## Chapter 2

# Neutral kaon physics

Neutral kaons are the lightest particles which contain a strange quark. Investigation of their properties gives an access to flavoured physics and allows to test  $\mathcal{CP}$ ,  $\mathcal{T}$  and  $\mathcal{CPT}$  symmetries. The  $\mathcal{CPT}$  symmetry assumes the invariance of physics phenomena under the combination of the discrete symmetries such as: charge conjugation ( $\mathcal{C}$ ), parity ( $\mathcal{P}$ ) and time reversal ( $\mathcal{T}$ ). One of possible ways to test the  $\mathcal{CPT}$  violation in neutral kaon system is to study the kaon semileptonic decay ( $K \rightarrow \pi e \nu$ ). Detailed description of this process is given in the following chapter.

### 2.1 Neutral kaon states

In 1947 Rochester and Butler discovered V-shaped tracks in a cloud-chamber during investigation of cosmic-ray showers [12]. Further studies showed that the lifetime of analyzed particles' was in the order of  $10^{-10}$  seconds (typical for weak interactions). To explain discrepancy in mode of production and decay a new quantum number was introduced by Gell-Mann [13] and Nishijima [14]. The symbol  $S$  and the name *strangeness* were introduced later.

Presently the strangeness in physics is associated with presence of the strange quark in a particle. In addition, strangeness is related to the electric charge ( $Q$ ), baryon number ( $B$ ) and the third component of the isospin ( $I_3$ ) by the phenomenological relation [15]:

$$S = 2Q - B - 2I_3. \quad (2.1)$$

Consequently, the particles that possess strangeness different from zero cannot decay into non-strange particles objects via interactions which conserve  $Q$ ,  $B$  and  $I_3$  (as strong interaction does). However, a pair of strange particles could be produced through strong interaction of non-strange particles (this is the so called "associated production"). An example of such pairs are:  $K^0, \bar{K}^0$  and  $B^0, \bar{B}^0$  mesons.

	$K^+$	$K^-$	$K^0$	$\bar{K}^0$
quarks	$u\bar{s}$	$\bar{u}s$	$d\bar{s}$	$d s$
strangeness	1	-1	1	-1

**Table 2.1:** Quark contents and strangeness of K mesons.

We can pair neutral and charged kaons into isospin doublets:  $(K^0, K^+)$  with  $S = 1$  and  $(K^-, \bar{K}^0)$  with  $S = -1$  (see Table 2.1). In 1955, Gell-Mann and Paris pointed out that  $K^0$  can turn into its antiparticle  $\bar{K}^0$ , through the sequence  $K^0 \rightarrow \pi^+\pi^- \rightarrow \bar{K}^0$  [16]. Consequently,  $K^0$  and  $\bar{K}^0$  are indistinguishable from the point of view of weak interactions. They also suggested that the flavour eigenstates of kaon could be presented as eigenstates of combined charge-parity ( $\mathcal{CP}$ ) symmetry [16]:

$$\begin{aligned} |K_+^0\rangle &= \frac{1}{\sqrt{2}} (|K^0\rangle + |\bar{K}^0\rangle), \\ |K_-^0\rangle &= \frac{1}{\sqrt{2}} (|K^0\rangle - |\bar{K}^0\rangle). \end{aligned} \quad (2.2)$$

where:

$$\begin{aligned} \mathcal{CP} |K_+^0\rangle &= + |K_+^0\rangle, \\ \mathcal{CP} |K_-^0\rangle &= - |K_-^0\rangle, \end{aligned} \quad (2.3)$$

However,  $|K_-^0\rangle$  and  $|K_+^0\rangle$  states are not identical with the observed hamiltonian eigenstates:  $|K_S\rangle$  and  $|K_L\rangle$ . Their properties and relations between each other will be presented in the further part of this work.

## 2.2 CP violation

Assuming conservation of the  $\mathcal{CP}$  symmetry, states  $|K_-^0\rangle$  and  $|K_+^0\rangle$  could decay into following channels:

$$\begin{aligned} \left. \begin{array}{l} |K_+^0\rangle \rightarrow \pi^+\pi^- \\ |K_+^0\rangle \rightarrow \pi^0\pi^0 \end{array} \right\} \mathcal{CP} = +1, \\ \left. \begin{array}{l} |K_-^0\rangle \rightarrow \pi^+\pi^-\pi^0 \\ |K_-^0\rangle \rightarrow \pi^0\pi^0\pi^0 \end{array} \right\} \mathcal{CP} = -1, \end{aligned}$$

and due to the large difference of the energy available for these decays a large difference in the life-times of  $K_-$  and  $K_+$  states is expected.

However, in 1964 Christenson, Cronin, Fitch and Turlay experimentally proved the violation of the  $\mathcal{CP}$  symmetry in weak interactions [17]. They observed the decay of the long lived state into two pions and established the frequency of this decay as:

$$\frac{N(K_L \rightarrow \pi^+\pi^-)}{N(K_L \rightarrow \text{all charged modes})} = (2.0 \pm 0.4) \times 10^{-3}. \quad (2.4)$$

Therefore, in order to properly describe the  $\mathcal{CP}$  violation, the hamiltonian eigenstates  $K_L$  and  $K_S$  are described as:

$$\begin{aligned} |K_L\rangle &= \frac{1}{\sqrt{2(1+|\epsilon_L|^2)}} \left( (1+\epsilon_L) |K^0\rangle - (1-\epsilon_L) |\bar{K}^0\rangle \right), \\ |K_S\rangle &= \frac{1}{\sqrt{2(1+|\epsilon_S|^2)}} \left( (1+\epsilon_S) |K^0\rangle + (1-\epsilon_S) |\bar{K}^0\rangle \right), \end{aligned} \quad (2.5)$$

where parameters  $\epsilon_L$  and  $\epsilon_S$  account for the symmetry violation. These parameters can be expressed in terms of  $\epsilon_K$  and  $\delta_K$  describing the  $\mathcal{CP}$  and  $\mathcal{CPT}$ , respectively:

$$\begin{aligned} \epsilon_S &= \epsilon_K + \delta_K, \\ \epsilon_L &= \epsilon_K - \delta_K. \end{aligned} \quad (2.6)$$

The above states ( $K_S, K_L$ ) are often called as a short and long-lived kaons. Their basic properties and main decay channels are shown in Table 2.2. A possible direct test of  $\mathcal{CP}$  or  $\mathcal{CPT}$  symmetries violation could be performed by measurement of the charge asymmetry in semileptonic decays of  $K_S$  and  $K_L$ , which will be presented in more details in the following sections.

	$K_S$		$K_L$	
mean life time	$(89.54 \pm 0.04)$ ps		$(51.16 \pm 0.21) \times 10^3$ ps	
mass	$497.614 \pm 0.024$ MeV/ $c^2$			
mass difference	$(3.484 \pm 0.006) \times 10^{-12}$ MeV/ $c^2$			
main branching ratios (BR)	$\pi^+\pi^-$	$(6.920 \pm 0.005) \times 10^{-1}$	$\pi^\pm e^\mp \nu_e$	$(4.055 \pm 0.011) \times 10^{-1}$
	$\pi^0\pi^0$	$(3.069 \pm 0.005) \times 10^{-1}$	$\pi^\pm \mu^\mp \nu_\mu$	$(2.704 \pm 0.007) \times 10^{-1}$
	$\pi^+\pi^-\gamma$	$(1.79 \pm 0.05) \times 10^{-3}$	$3\pi^0$	$(1.952 \pm 0.012) \times 10^{-1}$
	$\pi^\pm e^\mp \nu_e$	$(7.04 \pm 0.08) \times 10^{-4}$	$\pi^+\pi^-\pi^0$	$(1.254 \pm 0.005) \times 10^{-1}$
	$\pi^\pm \mu^\mp \nu_\mu$	$(4.69 \pm 0.05) \times 10^{-4}$	$\pi^\pm e^\mp \nu_e \gamma$	$(3.79 \pm 0.06) \times 10^{-3}$
			$\pi^+\pi^-$	$(1.966 \pm 0.010) \times 10^{-3}$
		$\pi^0\pi^0$	$(8.64 \pm 0.06) \times 10^{-4}$	

**Table 2.2:** Main properties of short and long-lived kaons [18].

### 2.3 Charge asymmetry in semileptonic decays of $K_S$ meson

According to the Standard Model, decay of  $K^0$  (or  $\bar{K}^0$ ) state is associated with the transition of the  $\bar{s}$  quark into  $\bar{u}$  quark (or  $s$  into  $u$ ) and emission of the charged boson. Change of strangeness ( $\Delta S$ ) implies the corresponding change of electric

charge ( $\Delta Q$ ) (see Figure 2.1). This is so called  $\Delta S = \Delta Q$  rule. Therefore, decay of  $K^0 \rightarrow \pi^- e^+ \nu$  and  $\bar{K}^0 \rightarrow \pi^+ e^- \bar{\nu}$  are present but  $K^0 \rightarrow \pi^+ e^- \bar{\nu}$  and  $\bar{K}^0 \rightarrow \pi^- e^+ \nu$  are not.

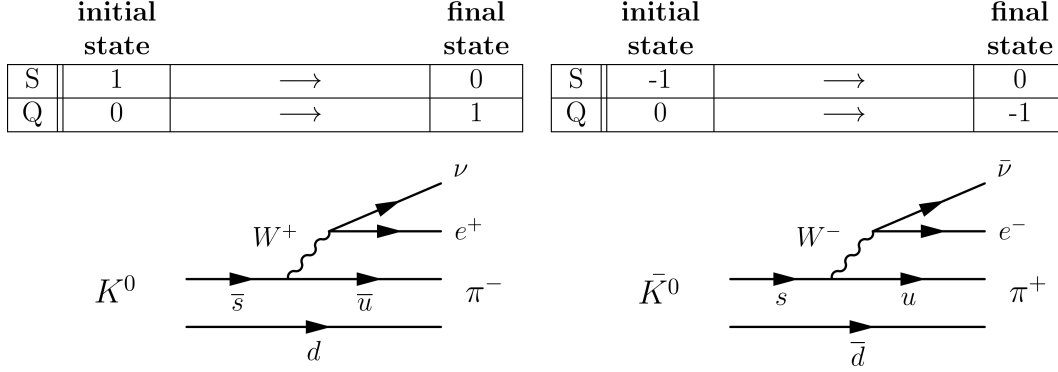


**Figure 2.1:** Feynman diagrams for  $K^0$  and  $\bar{K}^0$  semileptonic decay.

Decay amplitudes for semileptonic decays of states  $|K^0\rangle$  and  $|\bar{K}^0\rangle$  can be written as follows:

$$\begin{aligned}
 \langle \pi^- e^+ \nu | H_{weak} | K^0 \rangle &= a + b \equiv \mathcal{A}_+, \\
 \langle \pi^+ e^- \bar{\nu} | H_{weak} | \bar{K}^0 \rangle &= a^* - b^* \equiv \bar{\mathcal{A}}_-, \\
 \langle \pi^+ e^- \bar{\nu} | H_{weak} | K^0 \rangle &= c + d \equiv \mathcal{A}_-, \\
 \langle \pi^- e^+ \nu | H_{weak} | \bar{K}^0 \rangle &= c^* - d^* \equiv \bar{\mathcal{A}}_+,
 \end{aligned} \tag{2.7}$$

where the  $H_{weak}$  is a part of Hamiltonian corresponding to the weak interaction and  $a, b, c, d$  parameters describe the semileptonic decay amplitudes. Matrix elements are equal to combination of above parameters and are denoted as  $\mathcal{A}_+$  and  $\mathcal{A}_-$ .

For further considerations, rules for applying symmetry operators to amplitudes of two spin zero systems  $A$  and  $B$  (and corresponding anti-systems  $\bar{A}$  and  $\bar{B}$ ) could be summarized as [19]:

$$\begin{aligned}
 \langle \mathcal{T}\mathbf{B} | \mathcal{T}H_{wk}\mathcal{T}^{-1} | \mathcal{T}\mathbf{A} \rangle &= (\langle \mathbf{B} | \mathcal{T}H_{wk}\mathcal{T}^{-1} | \mathbf{A} \rangle)^* \\
 \langle \mathcal{C}\mathcal{P}\mathbf{B} | \mathcal{C}\mathcal{P}H_{wk}\mathcal{C}\mathcal{P}^{-1} | \mathcal{C}\mathcal{P}\mathbf{A} \rangle &= \langle \bar{\mathbf{B}} | \mathcal{C}\mathcal{P}H_{wk}\mathcal{C}\mathcal{P}^{-1} | \bar{\mathbf{A}} \rangle \\
 \langle \mathcal{C}\mathcal{P}\mathcal{T}\mathbf{B} | \mathcal{C}\mathcal{P}\mathcal{T}H_{wk}\mathcal{C}\mathcal{P}\mathcal{T}^{-1} | \mathcal{C}\mathcal{P}\mathcal{T}\mathbf{A} \rangle &= (\langle \bar{\mathbf{B}} | \mathcal{C}\mathcal{P}\mathcal{T}H_{wk}\mathcal{C}\mathcal{P}\mathcal{T}^{-1} | \bar{\mathbf{A}} \rangle)^*
 \end{aligned} \tag{2.8}$$

One obtains the relation between the semileptonic amplitudes and conservation of a particular symmetry by applying the presented above rules to the states (2.7). These considerations are summarized in Table 2.3.

Conserved quantity	Required relation
$\mathcal{T}$ symmetry	$Im(a) = Im(b) = Im(c) = Im(d) = 0$
$\mathcal{CP}$ symmetry	$Im(a) = Re(b) = Im(c) = Re(d) = 0$
$\mathcal{CPT}$ symmetry	$b = d = 0$
$\Delta S = \Delta Q$ rule	$c = d = 0$

**Table 2.3:** Relations between discrete symmetries and semileptonic amplitudes.

To simplify discussion it is useful to introduce the following notation [19, 20]:

$$\begin{aligned}
x &= \frac{\bar{\mathcal{A}}_+}{\mathcal{A}_+} = \frac{c^* - d^*}{a + b}, \\
\bar{x} &= \left(\frac{\mathcal{A}_-}{\bar{\mathcal{A}}_-}\right)^* = \frac{c^* + d^*}{a - b}, \\
y &= \frac{\bar{\mathcal{A}}_-^* - \mathcal{A}_+}{\bar{\mathcal{A}}_-^* + \mathcal{A}_+} = -\frac{b}{a}, \\
x_{\pm} &= \frac{x \pm \bar{x}^*}{2}.
\end{aligned} \tag{2.9}$$

The above quantities depend on  $\mathcal{CPT}$  symmetry and  $\Delta S = \Delta Q$  rule as presented in Table 2.4.

		$\Delta S = \Delta Q$	
		conserved	not-conserved
$\mathcal{CPT}$	conserved	$x = \bar{x} = 0$ $x_+ = x_- = 0$ $y = 0$	$x = \bar{x} \neq 0$ $x_+ \neq 0 \quad x_- = 0$ $y = 0$
	not conserved	$x \neq 0 \quad \bar{x} \neq 0$ $x_+ = x_- = 0$ $y \neq 0$	$x \neq 0 \quad \bar{x} \neq 0$ $x_+ \neq 0 \quad x_- \neq 0$ $y \neq 0$

**Table 2.4:** First order dependencies of  $\mathcal{CPT}$  symmetry and  $\Delta S = \Delta Q$  rule on amplitudes of semileptonic decays of K mesons

Quantities from equations (2.9) can be associated to the  $K_S$  and  $K_L$  semileptonic decay widths through the charge asymmetry ( $A_{S,L}$ ):

$$\begin{aligned}
A_{S,L} &= \frac{\Gamma(K_{S,L} \rightarrow \pi^- e^+ \nu) - \Gamma(K_{S,L} \rightarrow \pi^+ e^- \bar{\nu})}{\Gamma(K_{S,L} \rightarrow \pi^- e^+ \nu) + \Gamma(K_{S,L} \rightarrow \pi^+ e^- \bar{\nu})} \\
&= 2 \left[ Re(\epsilon_{S,L}) + Re\left(\frac{b}{a}\right) \mp Re\left(\frac{d^*}{a}\right) \right] \\
&= 2 [Re(\epsilon_{S,L}) - Re(y) \pm Re(x_-)].
\end{aligned} \tag{2.10}$$

Above equation contains only the first order of symmetry-conserving terms with parameters  $\epsilon_S, \epsilon_L$  (2.5) which can be expressed in terms of the  $\mathcal{CP}$  and  $\mathcal{CP}\mathcal{T}$  violation parameters  $\epsilon_K$  and  $\delta_K$  (2.6). The difference between the  $A_S$  and  $A_L$  is related to:

$$\begin{aligned} A_S - A_L &= 4\text{Re}(\delta_K) - 4\text{Re}\left(\frac{d^*}{a}\right) \\ &= 4\text{Re}(\delta_K) + 4\text{Re}(x_-). \end{aligned} \quad (2.11)$$

However, if the  $\Delta S = \Delta Q$  rule is conserved then the above equation simplifies to  $A_S - A_L = 4\text{Re}(\delta_K)$  (see Table 2.4). The  $A_L$  asymmetry is measured with a high precision  $A_L = (3.322 \pm 0.058_{\text{stat}} \pm 0.047_{\text{syst}}) \cdot 10^{-3}$  [7]. Therefore a precise measurement of the number of  $K_S$  semileptonic decays allows to determine the value of charge asymmetry and tests  $\mathcal{CP}\mathcal{T}$  symmetry and  $\Delta S = \Delta Q$  rule violation.

### 2.3.1 Experimental verification

#### $\Delta S = \Delta Q$ rule

In Standard Model the weak interactions violate conservation of the hadronic flavor and allow transition of one quark into another with different flavor. In case of strange particles the change of the strangeness is equal to the charge change. The most precise test of this  $\Delta S = \Delta Q$  rule was performed by KLOE collaboration by determination of  $\text{Re}(x_+)$  value in  $K_S$  semileptonic decays. Analysis was performed using data sample collected in 2001-2002 which corresponds to total luminosity of  $410 \text{ pb}^{-1}$ . Obtained result  $\text{Re}(x_+) = (-1.2 \pm 3.6) \times 10^{-3}$  [8] is consistent with zero which indicates conservation of  $\Delta S = \Delta Q$  rule (see Table 2.4).

#### Charge asymmetry

The charge asymmetry for  $K_L$  decays was precisely determined in KTeV experiment in Fermilab [7]. The measurement was based on 1.9 millions  $K_L \rightarrow \pi^\pm e^\mp \nu$  decays produced in collision of proton beam with BeO target.

Parameter	Most precise value	Reference	Collaboration
$A_S$	$(1.5 \pm 9.6_{\text{stat}} \pm 2.9_{\text{syst}}) \cdot 10^{-3}$	[8]	KLOE
$A_L$	$(3.322 \pm 0.058_{\text{stat}} \pm 0.047_{\text{syst}}) \cdot 10^{-3}$	[7]	KTeV
$\text{Re}(\delta_K)$	$(3.0 \pm 3.3_{\text{stat}} \pm 0.6_{\text{syst}}) \cdot 10^{-4}$	[21]	CPLEAR
$\text{Re}(x_+)$	$(-1.2 \pm 3.6) \cdot 10^{-3}$	[8]	KLOE
$\text{Re}(x_-)$	$(-0.8 \pm 2.5) \cdot 10^{-3}$	[8]	KLOE
$\text{Re}(y)$	$(0.4 \pm 2.5) \cdot 10^{-3}$	[8]	KLOE

**Table 2.5:** Summary of experimental parameters used to describe neutral kaon meson properties presented in the text.

At present the most accurate measurement of  $K_S$  charge asymmetry was conducted by KLOE collaboration [8]. Obtained charge asymmetry for  $K_S$  decays is consistent

in error limits with charge asymmetry for  $K_L$  decays (Table 2.5) suggesting conservation of  $\mathcal{CPT}$  symmetry. However, the accuracy of  $K_S$  determination is more than two orders of magnitude worse than this of the  $A_L$  determination and the error of  $A_S$  is dominated by a statistical uncertainty, which is three times larger than systematic. In this work we describe a new measurement of  $A_S$  based on about four times bigger data sample collected by the means of the KLOE detector in 2004-2005.



## Chapter 3

# KLOE experiment at DAΦNE

The idea of  $e^+e^-$  collider that would operate at energy equal to  $\phi$  meson mass was born in 1989 and two years later a proposal to create detector which would allow to investigate main  $\phi$  decay channels and study discrete symmetries was put forward [22, 23].

K LOng Experiment (KLOE) was mounted at DAΦNE in 1999 and collected data during two campaigns in 2001-2002 and 2004-2005. The gathered data sample corresponds to the total luminosity of  $2.5 \text{ fb}^{-1}$ . During last years the KLOE system was upgraded with three new sub-detectors (Inner Tracker [24], Quadrupole Calorimeter with Tiles [25] and Crystal Calorimeter with Timing [26]) and data taking campaign of KLOE-2 has started.

### 3.1 DAΦNE collider

DAΦNE is an  $e^+e^-$  collider located in the National Laboratory in Frascati (LNF) of National Institute of Nuclear Physics (INFN). The collider is designed to work in a center-of-mass energy at the mass of the  $\phi$  meson ( $\sqrt{s} \approx m_\phi$ ) which explains the common name of DAΦNE - the  $\phi$  factory.

The collider consists of two separate rings in which up to 120 bunches of electrons and positrons are stored. Each bunch contains about  $8.9 \times 10^{10}$  particles and interacts with its counterpart once per turn [27]. Electrons and positrons are accelerated to the desired energy in linac, stored and cooled in the accumulator before being injected into the rings.

Beams collide at two interaction regions (one for the KLOE and the other for FIN-

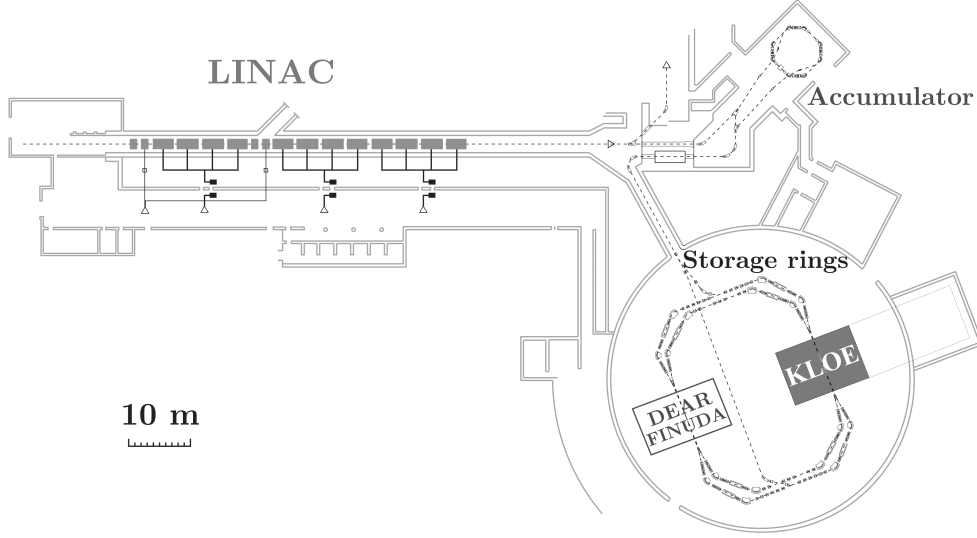


**Figure 3.1:** Schematic view of the DAΦNE collider. Electrons are accelerated in linac and after that directly transferred into accumulator or used for positron production on metallic target. In accumulator  $e^-$  and  $e^+$  beams are formed into bunches and injected into the storage rings with two intersection points where dedicated detectors collected data from collisions. Figure adapted from [27].

UDA<sup>1</sup>, DEAR<sup>2</sup> and SIDDHARTA<sup>3</sup> experiments) with a minimum bunch crossing period of:

$$T_{bunch} = 2.715 \text{ ns.} \quad (3.1)$$

Beams collide at the KLOE interaction point at a small angle of  $(\pi - 0.025)$  rad. As a result the produced  $\phi$  meson possess small average momentum along the x axis:

$$P_{\phi} = 13.1 \text{ MeV,} \quad (3.2)$$

corresponding to velocity  $\beta_{\phi} \sim 0.015$ .

Low- $\beta$  quadrupoles at interaction regions focus both beams to reach a luminosity of  $5 \times 10^{32} \text{ cm}^{-2}\text{s}^{-1}$ . A schematic view of the DAΦNE complex is shown in Figure 3.1 and detailed parameters are collected in Table 3.1.

<sup>1</sup>Fisica Nucleare a DAΦNE - for hypernuclear spectroscopy [28]

<sup>2</sup>DAΦNE Exotic Atom Research - for the spectroscopy of K-mesic hydrogen atoms [29]

<sup>3</sup>Silicon Drift Detectors for Hadronic Atom Research by Timing Application [30]

Bunch energy		0.51 GeV
Maximum luminosity		$5.3 \times 10^{32}$
Trajectory length		97.69 m
Minimum bunch separation		81.4 cm
RF frequency		368.25 MHz
Particles/bunch		$8.9 \cdot 10^{10}$
Bunch size	$\sigma_x$	0.02 cm
	$\sigma_y$	0.002 cm
	$\sigma_z$	3 cm
Synchr. radiation loss		9.3 keV/turn

**Table 3.1:** DAΦNE collider parameters [27].

## 3.2 KLOE detector

DAΦNE collider produce  $\sim 1300$  kaon pairs per second which corresponds to the luminosity  $5 \times 10^{32} \text{ cm}^{-2} \text{ s}^{-1}$ . A dedicated detector was needed for precise studies of the properties of  $\phi$  progeny particles (main decay channels of the  $\phi$  meson are presented in Table 3.2). Due to that, in 1991 the KLOE Collaboration was created and the detector was designed, tested and placed in one of DAΦNE interaction regions in 1999.

Decay channel	Branching ratio [%]
$\phi \rightarrow K^+ K^-$	$48.9 \pm 0.5$
$\phi \rightarrow K_S K_L$	$34.2 \pm 0.4$
$\phi \rightarrow \rho\pi + \pi^+ \pi^- \pi^0$	$15.32 \pm 0.32$
$\phi \rightarrow \eta\gamma$	$1.309 \pm 0.024$

**Table 3.2:** Main decays modes of the  $\phi$  meson [18].

The KLOE detector was designed to carry out a wide-ranging program in neutral and charged kaon physics and to measure properties of scalar and pseudoscalar mesons. In this thesis a particular emphasis will be given to  $\phi$  decay channel with so called K-short ( $K_S$ ) and K-long ( $K_L$ ) states (Chapter 2). The size of the KLOE detector was optimized for efficient detection of the  $K_L$  mesons. A 2 m radius of a drift chamber allows to register about 40% of  $K_L$  decays inside the chamber while the rest reach the electromagnetic calorimeter. A schematic cross-section side view of the KLOE detector is shown in Figure 3.2. The main components of KLOE are the cylindrical drift chamber and the calorimeter, both surrounding the beam pipe. A detailed description is given in next subsections of this thesis. All elements are immersed in a 0.52 T magnetic field created by superconducting coils that are placed along the beam axis. Since time measurement by means of calorimeter is crucial for Time of Flight method applied in this analysis (Chapter 4), detailed description of

time determination is given in the subsection devoted to calorimeter.

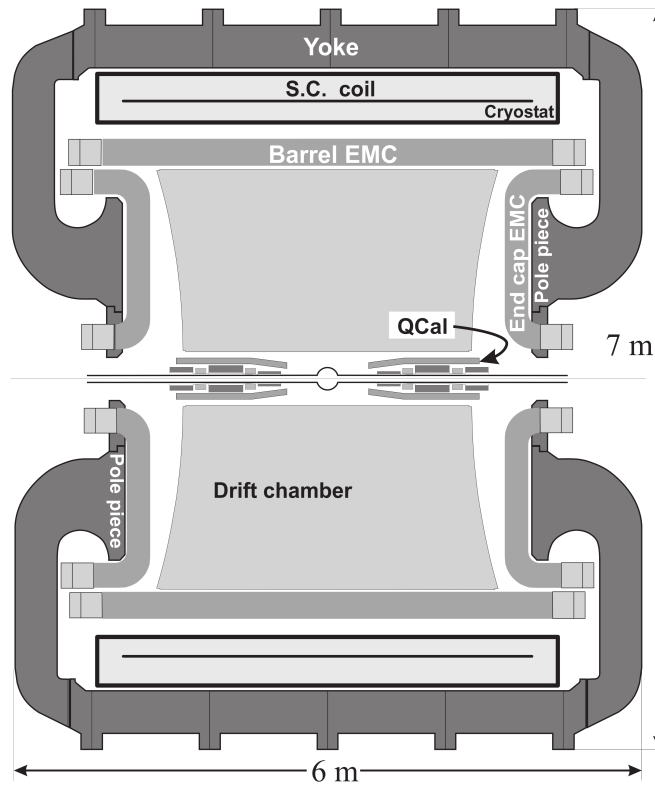


**Figure 3.2:** Scheme of the KLOE detector system. Drift chamber in the central part of the KLOE detector is surrounded by the electromagnetic calorimeter. Both detectors are inserted in a magnetic field (0.5 T). Additional QCALT calorimeters are mounted around a beam pipe. Figure adapted from [27].

### 3.2.1 The drift chamber

The KLOE drift chamber (DC) is a 3.3 m long cylinder with an internal and external radii of 25 cm and 2 m, respectively. Between the endplates around 12500 sense wires are stretched. The rest of the wires ( $\sim 39500$ ) are used to form an electric field in the DC. All wires are gathered in 60 layers – the 12 innermost layers make up  $2 \times 2$  cm<sup>2</sup> cells and the remaining 48 layers  $3 \times 3$  cm<sup>2</sup> cells. In order to define the position on the  $z$  axis the wires in neighboring layers are twisted in opposite directions by a small  $\epsilon$  angle (Figure 3.3). The value of this angle is changing with the radius and takes values between 60 and 150 mrad. The efficiency of detecting a charged particle in a cell is  $\sim 99.6$  % [23].

To minimize the  $K_L \rightarrow K_S$  regeneration in the DC two solutions have been applied:

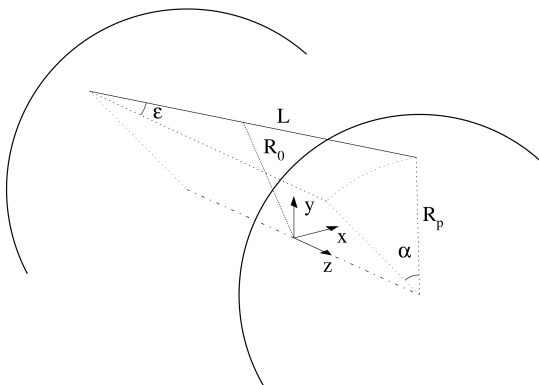


**Figure 3.3:** Schematic view of the geometry of the  $z$  wire stretching that length is equal  $L$ . Wires from the consecutive layers have alternating signs of stereo angle  $\epsilon$  which allows to determine the  $z$  coordinate of the hit. The value of the angle  $\alpha$  has been chosen to obtain a constant value of difference between  $R_0$  and  $R_p$  independently of the absolute radius. Figure is adapted from [27].

the DC walls are composed of low-density materials: carbon fiber and epoxy and a gaseous mixture of isobutane (10%) and helium (90%) is used to fill out the chamber. Such mixture is characterised by small density even though it has a higher diffusion coefficient than other gases [23].

Particle path and associated vertices in detector are reconstructed in the following steps:

- neighboring hits are tied into single track - a first estimation of a track parameters is given,
- obtained track parameters are improved by applying the track fit,
- by taking into account the smallest distance between tracks the position of primary and secondary vertices is evaluated.

The described procedure allows to obtain a spatial resolution in the  $r, \varphi$  plane better than  $200 \mu\text{m}$ , a resolution along the  $z$  axis of  $\sim 2 \text{ mm}$  and on the decay vertex position of  $\sim 1 \text{ mm}$ . Moreover, the curvature of the reconstructed tracks allows to determine the particle momentum with a relative accuracy of  $\frac{\sigma(p)}{p} = 0.4 \%$ .

### 3.2.2 The calorimeter

The drift chamber allows to reconstruct information about charged particles while the calorimeter enables recording of both charged and neutral particles. The KLOE calorimeter has been designed to have an excellent accuracy of energy determination

and time resolution in order to register the hits of neutral particles and provide a possibility of the Time of Flight (TOF) measurement.

The calorimeter is composed of 24 modules with trapezoidal cross-section that forms a barrel-shaped component and 32 additional modules which form two endcaps closing the barrel (Figure 3.2). The endcaps are composed of modulus with rectangular cross section wrapped around the pole pieces of the magnet yoke into C-shapes. The above described structure of the calorimeter covers up to  $\sim 98\%$  of the solid angle around the interaction point and allows to avoid dead zones between barrel and endcaps.

The composition of each module is a mixture of [27]:

- lead (48%) which enhances the electromagnetic shower production,
- scintillating fibers (42%) with a diameter of 1 mm and light propagation of  $\sim 17\text{cm/ns}$  (for 1 MeV of deposited energy more than  $5 \times 10^3$  photons are produced),
- glue (10%),

which allows to obtain an average density of  $5\text{g} \cdot \text{cm}^{-3}$  and the radiation length  $X_0$  of about 1.5 cm. Array of photomultipliers at the ends of scintillator strips is used for light collection. This design divides each module into 5 planes and 12 columns of readout segments (cells). When particle passes through the calorimeter its energy is deposited in one or more cells. During the event analysis those cells are grouped into clusters. The sum of energy in those cells allows to reconstruct particle energy. The distribution of those cells weighted by energy allows to determine the hit position with a resolution of  $\sigma_x = \sigma_y = 1.3\text{ cm}$  [27], while obtained energy resolution at KLOE EMC scales as [23]:

$$\frac{\sigma(E)}{E} = \frac{5.4\%}{\sqrt{E[\text{GeV}]}}. \quad (3.3)$$

The signal arrival time recorded in both photomultiplier tubes ( $t^A$  and  $t^B$ ) consist of the arrival time of a hit ( $t^{cell}$ ) and time of a light signal traveling from the hit point to the ends of the scintillator ( $t_L^A$  and  $t_L^B$ ), which could be summarized in the following equation (for simplicity the cable delays are omitted):

$$t^{A,B} = t_L^{A,B} + t^{cell}. \quad (3.4)$$

Using the information about the module length ( $L$ ) and light velocity ( $v$ ) one can retrieve information about the time of the hit:

$$t^{cell} = \frac{t^A + t^B}{2} - \frac{t_L^A + t_L^B}{2} = \frac{t^A + t^B}{2} - \frac{L}{2v}. \quad (3.5)$$

The time resolution is obtained by the analysis of various radiative  $\phi$  decays and is equal to [23]:

$$\sigma_t = \frac{54\text{ ps}}{\sqrt{E[\text{GeV}]}} \oplus 140\text{ ps}. \quad (3.6)$$

The  $z$  coordinate is obtained from:

$$z^{cell} = \frac{t_L^B - t_L^A}{2} \cdot v, \quad (3.7)$$

while resolution of the  $z$  coordinate determination is expressed as [23]:

$$\sigma_z = \frac{1.2\text{cm}}{\sqrt{E[\text{GeV}]}}. \quad (3.8)$$

The cluster time and  $z^{clu}$  coordinate of a whole cluster are calculated as energy-weighted average from grouped cells and  $z^{cell}$  coordinates, respectively.

In general case time ( $t$ ) measured in the calorimeter is defined as:

$$t = t^{TOF} + t^{offset} - n \times T_{bunch}, \quad (3.9)$$

where the  $t^{TOF}$  is the time of flight of particle from interaction point to the calorimeter,  $t^{offset}$  denotes delays due to the signal propagation in the modules and electronics and  $T_{bunch}$  is the bunch crossing period (Eq. 3.1). The number  $n$  is estimated by assuming that the first cluster is generated by a first photon that reach the calorimeter (prompt photon). This cluster is called the  $T_0$ -cluster and the global offset of the event is given by:

$$T_0 = t^{offset} - n \times T_{bunch}, \quad (3.10)$$

and needs to be estimated event by event and subtracted from all times recorded in calorimeter.



## Chapter 4

# Registration of the $\phi \rightarrow K_L K_S \rightarrow K_L e^\pm \pi^\mp \nu$ process at KLOE

Neutral kaons from  $\phi$  decays are produced in pairs and this property is used in so-called tagging technique - identification of  $K_L$  ( $K_S$ ) meson on one side allows to select a  $K_S$  ( $K_L$ ) meson on the other side of  $\phi$  decay point. Identification procedure is simplified by the difference in  $K_L$  and  $K_S$  mesons mean life times -  $K_S$  decays close to the interaction point therefore in the analysis a position of  $K_L$  vertex can be limited to distances larger than  $\sim 15$  cm from the interaction point.

Analysis described in this thesis is based on an identification of  $K_S$  through the detection of  $K_L$  interaction in the calorimeter. In order to select semileptonic decays of  $K_S$  mesons, an additional kinematic selection is applied. It starts from a requirement of a vertex formation by tracks of two oppositely charged particles near the interaction point. Those tracks must be associated to calorimeter clusters. Obtained tracks parameters allows identification of charged particles in a final state by applying the Time of Flight technique.

### 4.1 $K_L$ measurement - $K_S$ tagging

About 60% of produced  $K_L$  mesons reach the calorimeter and deposit up to 497 MeV energy (so called  $K_L$  *crash*). Due to that, the selection of  $K_L$  candidates takes into account only clusters with energy  $E_{clu}(K_{crash})$  higher than 100 MeV. It is also required that the cluster is not close to any track reconstructed in drift chamber. Obtained energy distribution of  $K_L$  *crash* is shown in Figure 4.1. The discrepancy between data (dashed histogram) and Monte Carlo (MC) simulations (thin, solid

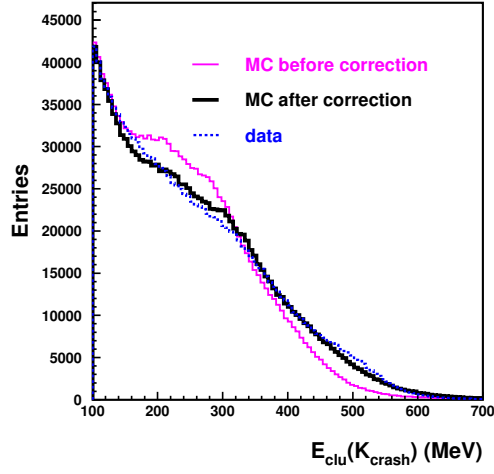


**Figure 4.1:** Distribution of  $K_L$  crash energy for data (dashed histogram) and Monte Carlo simulations before (thin solid histogram) and after (thick solid histogram) making correction described in text.

histogram) due to simplified description of calorimeter in MC simulation is visible. Therefore, the energy distribution was modified by the phenomenological correction:

$$E_{clu}^{new}(K_{crash}) = E_{clu}^{old}(K_{crash}) \cdot (p1 + Int(E_{clu}^{old} - 100) \cdot p2), \quad (4.1)$$

where  $E_{clu}^{old}(K_{crash})$  and  $E_{clu}^{new}(K_{crash})$  stands for cluster energy before and after making correction, while values of  $p1$  and  $p2$  were obtained from previous KLOE analysis and are equal to 1.025 and 0.0003, respectively [31]. The final result is shown in Figure 4.1.

Since, angular distributions of kaons emission is described by characteristic p-wave angular distribution:

$$\frac{dN}{d\Omega} \propto \sin^2 \theta, \quad (4.2)$$

where  $\theta$  is a polar angle, most of kaons are emitted in the direction perpendicular to the  $z$  axis. Therefore, part of background can be rejected by choosing  $K_L$  clusters only in the barrel.

In the next step, for each cluster candidate the velocity of contributing particle is calculated as:

$$\beta_{clu} = \frac{R_{clu}}{c \cdot t_{clu}}, \quad (4.3)$$

where  $R_{clu}$  and  $t_{clu}$  denote a distance and time of flight of the  $K_L$  between the interaction point and cluster position respectively, and  $c$  is the speed of light. In the  $\phi$  meson rest frame  $K_L$  mesons possess low velocity  $\beta \sim 0.22$ . To compare obtained

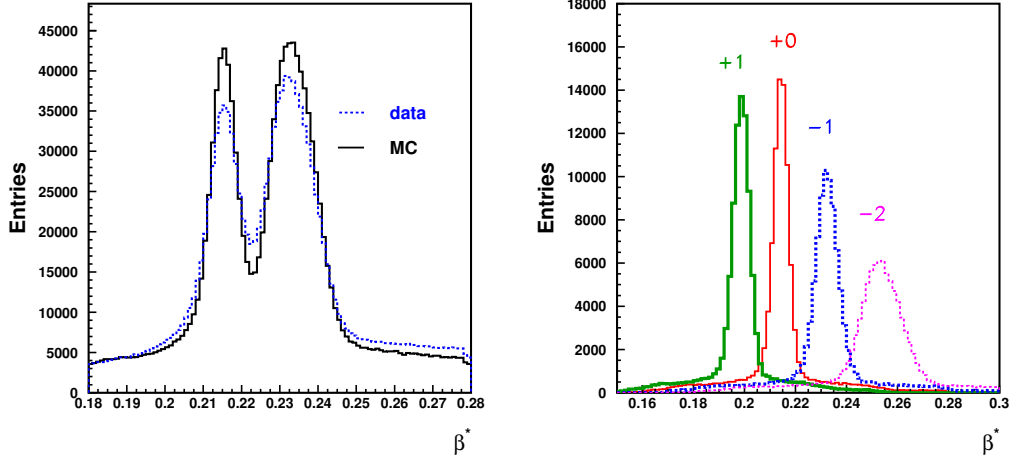


**Figure 4.2:** Distribution of velocity of the tagging  $K_L$  meson obtained in analysis and by imposing the different bunch number ( $n$  value) in MC simulations are shown on left and right picture, respectively. Left figure shows comparison of experimental and simulated histograms (explanation of double peak structure is given in the text), whereas right figure shows results of simulations.

$\beta_{clu}$  value with the theoretical one the transformation to the  $\phi$  rest frame is applied:

$$\beta^* = \frac{\sqrt{\beta_{clu}^2 + \beta_\phi^2 + 2\beta_{clu}\beta_\phi \sin \theta \cos \phi'}}{1 - \beta_\phi \beta_{clu} \sin \theta \cos \phi'}, \quad (4.4)$$

where  $\beta_\phi$  is a nominal  $\phi$  meson velocity to be  $1.27 \times 10^{-2}$  at the energy of DAΦNE, while  $\theta$  and  $\phi'$  are polar and azimuthal angles, respectively, between the  $\phi$  meson momentum vector and direction connecting the interaction point with the cluster position.

The obtained  $\beta^*$  distribution (Figure 4.2, left) peaks at two different values due to the procedure used to determine a  $T_0$  (described in subsection 3.2.2), which assumes first cluster to be generated by a prompt photon which does not occur while investigating the semileptonic decays. If the  $T_0$ -cluster is generated by the fastest pion, which has a time of flight of  $\sim 10$  ns (instead of 6 – 7 ns for prompt photon), then the  $n$  value defined in Eq. 3.10 differs from the correct value by (-1). Example of simulated  $\beta^*$  distribution for different  $n$  values is shown in Figure 4.2, right. Hence the applied cut  $0.17 < \beta^* < 0.28$  is chosen to contain both peaks, for further analysis.

If more than one cluster fulfilled above criteria then the one with smallest time of arrival ( $t_{clu}$ ) is chosen as corresponding to the interaction of the  $K_L$  meson.

## 4.2 $K_S$ identification

Identification of  $K_L$  interaction in the calorimeter allows to tag the short lived kaon on the other side of the  $\phi$  meson decay point. In the next step, the signals from drift chamber and Time of Flight technique are applied to improve signal over background ratio and to identify registered particles.

### 4.2.1 $K_S \rightarrow \pi e \nu$ events preselection

A sketch of typical  $K_S \rightarrow \pi e \nu$  event is shown in Figure 4.3 (left). Selection of semileptonic events starts from requirement of two oppositely charged particles with tracks forming a vertex close to the interaction point (IP):

$$\begin{aligned} \rho_{vtx} &< 15 \text{ cm}, \\ |z_{vtx}| &< 10 \text{ cm}, \end{aligned} \quad (4.5)$$

where  $\rho_{vtx} = \sqrt{x_{vtx}^2 + y_{vtx}^2}$ . Obtained distribution is shown in Figure 4.3 (right).

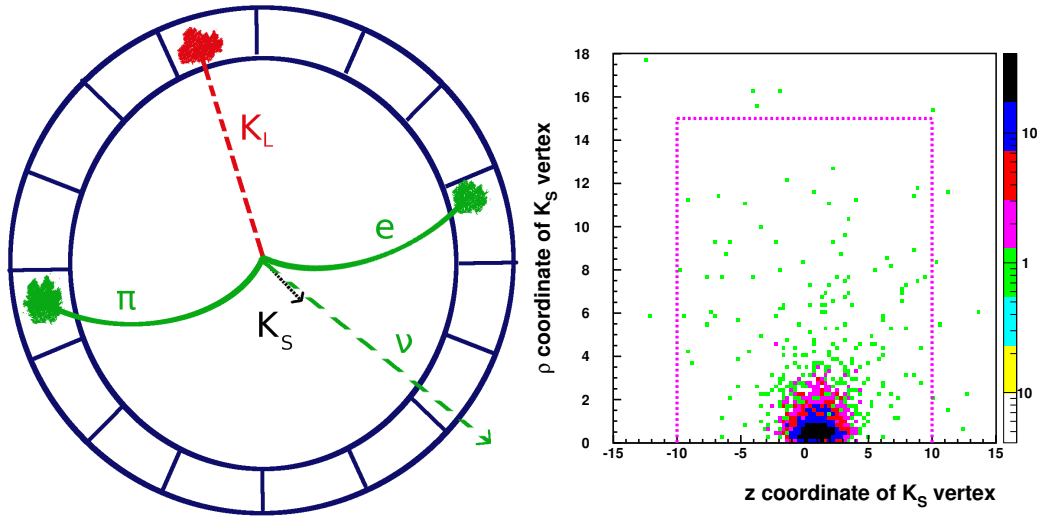


**Figure 4.3:** Left: Transverse view of exemplary signal event. The  $K_S$  is identified using the  $K_L$  interaction in the calorimeter. In the next step two oppositely charged particle tracks that form a vertex near the interaction point are selected. Both tracks must be associated with the calorimeter cluster. Right: Monte Carlo simulation of radial and  $z$  coordinates of vertex position for  $K_S \rightarrow \pi e \nu$  events. Dashed line represents applied cuts which preserves  $\sim 95\%$  of the signal (as it is visible the Interaction Point is not at the beginning of reference frame).

The  $K_S \rightarrow \pi^+ \pi^-$  decays with  $\text{BR} \sim 10^4$  larger than the signal constitute the main background source for the identification of  $K_S \rightarrow \pi e \nu$  decays, due to the possible misidentification of  $\pi$  and  $e$ .

Main cuts to reject  $K_S \rightarrow \pi^+\pi^-$  events at preselection stage are:

- $70^\circ < \alpha < 175^\circ$

where  $\alpha$  is an angle between charged secondaries in  $K_S$  rest frame. Obtained  $\alpha$  distribution is shown on the left side of Figure 4.4. In case of two body decay (such as  $K_S \rightarrow \pi^+\pi^-$ )  $\alpha$  takes value  $\sim 180^\circ$  and in case of three body decay ( $K_S \rightarrow \pi e \nu$ ) it is spanned over a large angle range (dashed histogram). Requirement of  $70^\circ < \alpha < 175^\circ$  allows to reduce the  $K_S \rightarrow \pi\pi$  background by 94% while only 4% of  $K_S \rightarrow \pi e \nu$  events is rejected.

- $300 < M_{inv} < 490$  MeV

an invariant mass  $M_{inv}$  is calculated using momenta of the particles which tracks form a vertex assuming that both particle were pions. Obtained distribution is shown on the right side of Figure 4.4. This requirement reduces remaining  $K_S \rightarrow \pi\pi$  decays by 53% while only 4% of signal is rejected.

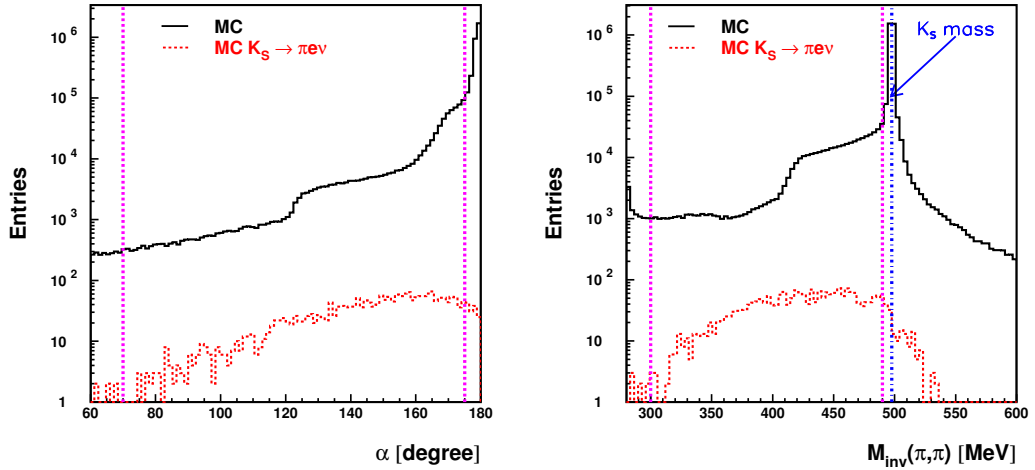


**Figure 4.4:** Left: Simulated distribution of angle between charged secondaries in  $K_S$  rest frame. Right: Simulated distribution of invariant mass calculated under assumption that both registered particles were pions. In both figures solid and dashed histograms represent all events and semileptonic decays, respectively. Vertical dashed lines represent cuts described in text.

Both tracks reconstructed in the drift chamber are associated with neighbouring clusters in calorimeter (TCA - Track to Cluster Association). TCA procedure extrapolates each of tracks from last registered position in drift chamber toward the calorimeter surface and determines the impact point. Neighbouring cluster is associated to the track when the transverse distance between the centroid position of the cluster and track impact point is smaller than 30 cm. Efficiencies after each step of preselection are presented in Table 4.1.

Efficiency	Efficiency components	$K_S$ decay		
		$\pi^- e^+ \nu$	$\pi^+ e^- \bar{\nu}$	$\pi^\pm \pi^\mp$
$\epsilon_1$	two oppositely charged particles	0.86961(80)	0.87023(80)	0.90029(15)
$\epsilon_2$	$ z_{vtx}  < 10$ cm	0.92497(67)	0.92588(66)	0.95084(12)
$\epsilon_3$	$\rho_{vtx} < 15$ cm	0.98528(31)	0.98514(32)	0.98846(59)
$\epsilon_4$	$70^\circ < \alpha < 175^\circ$	0.96656(48)	0.96620(48)	0.16376(21)
$\epsilon_5$	$300 < M_{inv} < 490$ MeV	0.96082(53)	0.96138(52)	0.47325(68)
$\epsilon_{DC}$	$\epsilon_{DC} = \epsilon_1 \epsilon_2 \epsilon_3 \epsilon_4 \epsilon_5$	0.7360(10)	0.7373(10)	0.0656(13)
$\epsilon_{TCA}$		0.4799(14)	0.4755(14)	0.6192(10)

**Table 4.1:** Summary for drift chamber selection and Track to Cluster Association (TCA) efficiencies. Statistical uncertainty for efficiency is calculated as binomial error [32].

#### 4.2.2 Particle identification with Time of Flight method

The Time of Flight technique aims at rejection of the background, which at this stage of analysis is due to  $K_S \rightarrow \pi^+ \pi^-$  events, and at identification of the final charge states ( $\pi^\pm e^\mp$ ). For each particle, the difference  $\delta_t$  between the measured time of associated cluster ( $t_{cl}$ ) and expected time of flight is calculated assuming a given mass hypothesis,  $m_x$ :

$$\delta_t(m_x) = t_{cl} - \frac{L}{c \cdot \beta(m_x)},$$

$$\beta(m_x) = \frac{P}{\sqrt{P^2 + m_x^2}},$$
(4.6)

where  $L$  is a total length of particle trajectory and  $P$  is particle momentum. Since  $T_0$  depend on unknown bunch number  $n$  (see Eq 3.9), an independent (on  $T_0$ ) difference of  $\delta_t(m_a)$  and  $\delta_t(m_b)$  is used:

$$d\delta_{t,ab} = \delta_t(m_a)_1 - \delta_t(m_b)_2.$$
(4.7)

In order to improve time measurement in Time of Flight technique the distance between the particle impact point on the calorimeter and the cluster centroid position was calculated. This correction was separately evaluated and applied to the data and Monte Carlo simulation after improving the agreement between simulation and data. Detailed description is presented in reference [33].

Two cuts are further applied. For the first cut, both particles are assumed to be pions and the following value is calculated:

$$d\delta_{t,\pi\pi} = \delta_t(m_\pi)_1 - \delta_t(m_\pi)_2,$$
(4.8)

for  $K_S \rightarrow \pi\pi$  events this value is around zero and this fraction of events could be rejected by requiring:

$$|d\delta_{t,\pi\pi}| > 1.5 \text{ ns.} \quad (4.9)$$

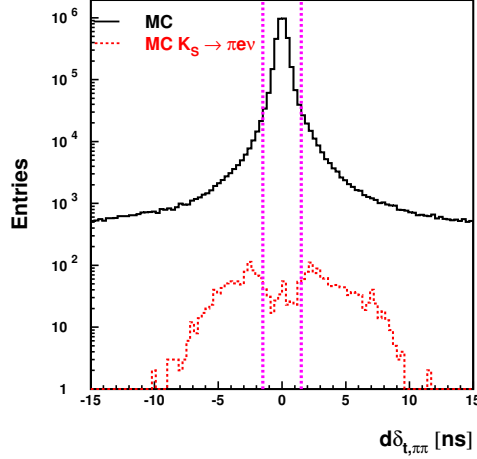


**Figure 4.5:** Simulated distribution of  $d\delta_{t,\pi\pi}$  for  $K_S \rightarrow \pi e \nu$  and all events. Vertical dashed lines represents cut described in text.

Then, for surviving events, the pion-electron hypothesis is tested:

$$\begin{aligned} d\delta_{t,\pi e} &= \delta_t(m_\pi)_1 - \delta_t(m_e)_2, \\ d\delta_{t,e\pi} &= \delta_t(m_e)_1 - \delta_t(m_\pi)_2. \end{aligned} \quad (4.10)$$

If a mass assumption is correct then one of the variables above should be close to zero. The obtained Monte Carlo distributions for  $K_S \rightarrow \pi^\pm e^\mp \nu$  and background events are presented in Figure 4.6. Hence, the following cut is applied:

$$\begin{aligned} |d\delta_{t,e\pi}| < 1.3 \text{ ns} \wedge d\delta_{t,\pi e} < -3.4 \text{ ns} \\ \text{or} \\ d\delta_{t,e\pi} > 3.4 \text{ ns} \wedge |d\delta_{t,\pi e}| < 1.3 \text{ ns} \end{aligned} \quad (4.11)$$

The above requirement ensures that the possibility of misidentification of charged particles from signal events is equal to  $10^{-4}$  only.

In the next step, using the mass assignment known from the cut defined in Eq. 4.10 the  $T_0$  is evaluated:

$$T_0 = N_{int} \left( \frac{\delta_t(m_\pi) + \delta_t(m_e)}{2 \cdot T_{bunch}} \right) \times T_{bunch}, \quad (4.12)$$

where  $N_{int}$  stands for the integer part and  $T_{bunch}$  is the minimum bunch crossing period (see Eq. 3.1 and Eq. 3.10). Obtained distributions of  $\delta_t(\pi)$  and  $\delta_t(e)$  before and after recalculating  $T_0$  are shown in Figure 4.7.

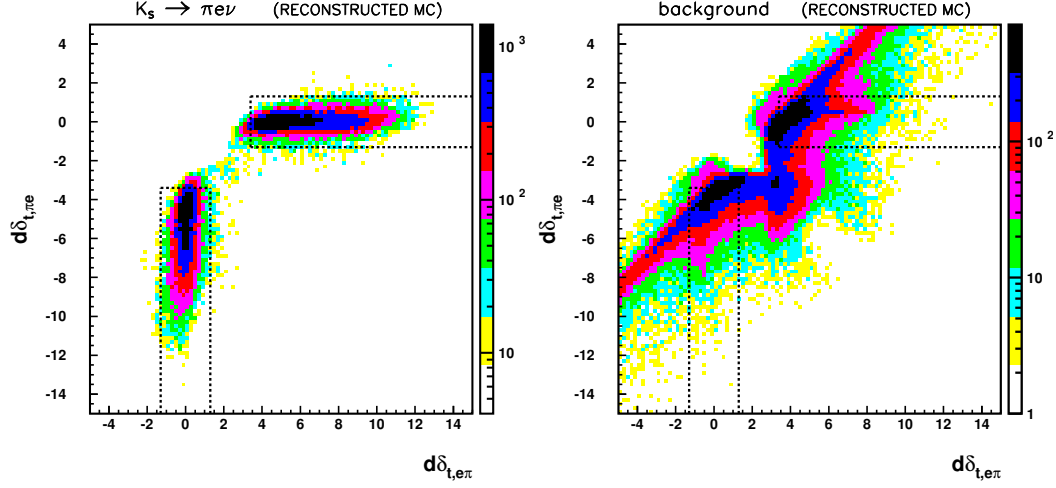


**Figure 4.6:** Simulated distributions of time differences  $d\delta_{t,\pi e}$  vs  $d\delta_{t,e\pi}$  defined in Eq. 4.10 for  $K_S \rightarrow \pi e \nu$  events (left) and background events (right), once the  $\delta_{t,\pi\pi}$  cut has been applied. The regions delimited by the dashed lines are selected. In case of  $e\pi$  ( $\pi e$ ) the  $d\delta_{t,e\pi}$  ( $d\delta_{t,\pi e}$ ) variable takes value close to zero.

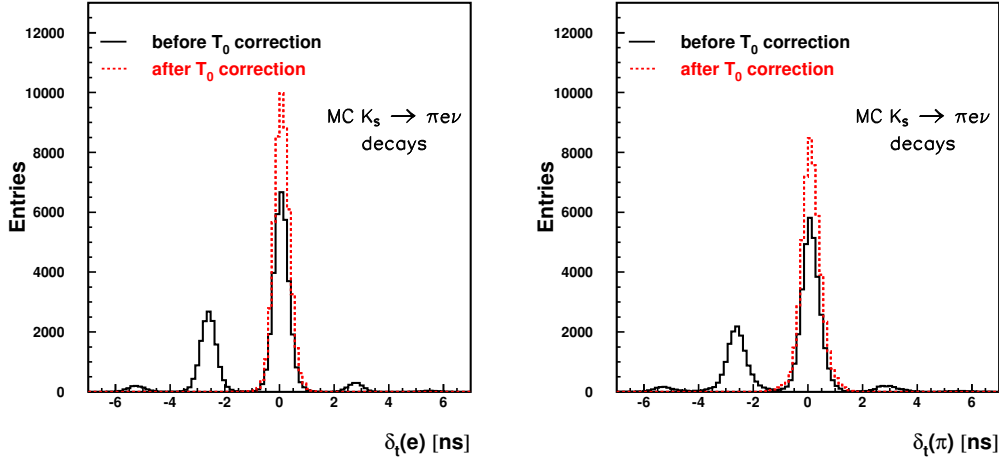


**Figure 4.7:** Distribution of  $\delta_t(e)$  (left) and  $\delta_t(\pi)$  (right) for  $K_S \rightarrow \pi e \nu$  events before (solid line) and after correcting the  $T_0$  value (dashed line). After particle identification  $T_0$  can be reevaluated and subtracted from particle arrival time registered in calorimeter.

Efficiency	Efficiency components	$K_S$ decay		
		$\pi^- e^+ \nu$	$\pi^+ e^- \bar{\nu}$	$\pi^\pm \pi^\mp$
$\epsilon_1$	$ d\delta_{t,\pi\pi}  > 1.5$ ns	0.94250(93)	0.93647(98)	0.29369(12)
$\epsilon_2$	$( d\delta_{t,e\pi}  < 1.3 \wedge d\delta_{t,\pi e} < -3.4)$ or $(d\delta_{t,e\pi} > 3.4 \wedge  d\delta_{t,\pi e}  < 1.3)$	0.92157(99)	0.94861(91)	0.24913(20)
$\epsilon_{TOF}$	$\epsilon_{TOF} = \epsilon_1 \epsilon_2$	0.8685(13)	0.8883(13)	0.0732(66)
$\epsilon_{CIRCLE}$		0.8757(14)	0.8975(13)	0.0816(26)

**Table 4.2:** Efficiency summary for both Time of Flight cuts described in section 4.2.2 and circle cut ( $\epsilon_{CIRCLE}$ ). Statistical uncertainty for efficiency is calculated as binomial error [32].

After particle identification and subtracting  $T_0$  from registered cluster times the time difference  $\delta_t(m_x)$  is reevaluated with the mass assignment known from the cut on  $d\delta_{t,e\pi}$  (Eq. 4.10). Obtained distributions for simulated data and experimental KLOE data are shown in Figure 4.8 (top). The Monte Carlo simulation indicate the signal position around the point (0,0) while the background location is spread at the corners of the obtained distribution. Due to that an additional TOF cut is applied by selecting events within the circle in the  $\delta_t(e)$  vs  $\delta_t(\pi)$  plane, as shown in Figure 4.8 (bottom). This cut allows to preserve 94% of the remaining signal and control the number of selected background events for normalization. Details of the normalization procedure are presented in next chapter. Efficiencies obtained at each step of analysis described in this chapter are shown in Table 4.2.

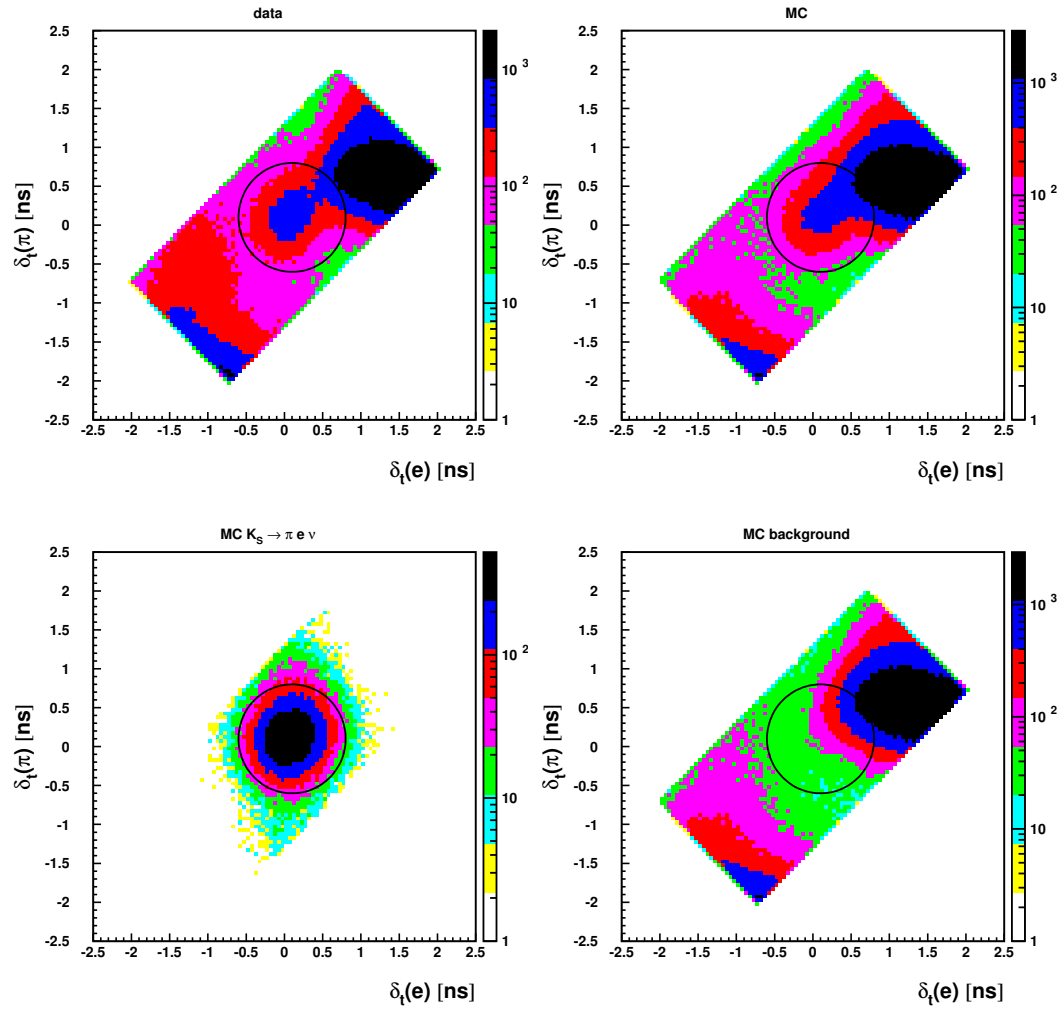


**Figure 4.8:** Distributions of the time difference for pion mass hypothesis ( $\delta_t(\pi)$ ) versus the time difference for electron mass hypothesis ( $\delta_t(e)$ ) for experimental data (top-left), total MC events (top-right), MC  $K_S \rightarrow \pi e \nu$  events (bottom-left) and MC background events (bottom-right). Events within the circle are retained for further analysis.

## Chapter 5

# Measurement of charge asymmetry for $K_S \rightarrow \pi^\mp e^\pm \nu(\bar{\nu})$ decay

In order to evaluate the number of events for final states  $\pi^\mp e^\pm \nu(\bar{\nu})$  the normalization procedure should be introduced. For this purpose, kinematic variables, that allows to discriminate between the main background contributions and  $K_S \rightarrow \pi e \nu$  events, will be introduced. Obtained information from normalization procedure combined with analysis efficiency allows to obtain the charge asymmetry for  $K_S$  semileptonic decay.

### 5.1 Normalization procedure

For studied  $K_S \rightarrow \pi e \nu$  decay only massless neutrino is not registered and the difference between the missing energy and momentum,  $\Delta E(\pi, e) = E_{miss}(\pi, e) - p_{miss}(\pi, e)$  should be close to zero and can be used for further suppression of background channels. The distribution of  $\Delta E(\pi e)$  is shown in Figure 5.1. The peak around zero is corresponding to a signal from  $K_S \rightarrow \pi e \nu$  events.

The background is dominated by the following decays:

- $K_S \rightarrow \pi^+ \pi^-$ , where one of the pion track is badly reconstructed and classified as electron by Time of Flight procedure,
- $K_S \rightarrow \pi \mu$ , are a subset of  $K_S \rightarrow \pi^+ \pi^-$  decays with condition that one of the pion decay into muon before entering the drift chamber,
- $K_S \rightarrow \pi^+ \pi^- \gamma$  where the photon radiated at  $K_S$  vertex carry away enough energy to shift the invariant mass  $M_{\pi, \pi}$  below 490 MeV and  $E_{miss}$  toward

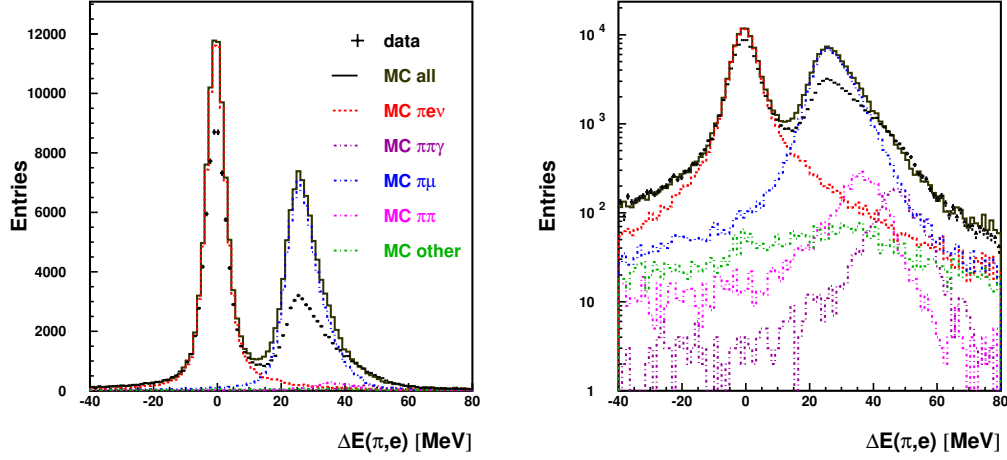


**Figure 5.1:** Distribution of  $\Delta E(\pi, e) = E_{miss} - p_{miss}$  for all selected events in linear (left) and logarithmic (right) scales before normalization. Points represents data from the entire data set, the solid lined represents all Monte Carlo simulation, dashed line stands for  $K_S \rightarrow \pi e \nu$  events and dashed-dotted line shows various background contributions.

positive values,

- other, mainly  $K_S \rightarrow \pi \mu \nu$  or  $\phi \rightarrow K^+ K^-$  decays.

A final sample contains more than one source of background and therefore for each background category dedicated kinematic criterium is used for its suppression:

$\Delta \mathbf{E}(\pi, e) = E_{miss}(\pi, e) - p_{miss}(\pi, e)$   
 difference between the missing energy and momentum calculated under assumption that particles are coming from semileptonic decay. In case of  $K_S \rightarrow \pi e \nu$  decay  $\Delta E(\pi, e)$  will take values around zero.

$\Delta \mathbf{E}(\pi, \pi) = E_{miss}(\pi, \pi) - p_{miss}(\pi, \pi)$   
 difference between the missing energy and momentum in  $\pi - \pi$  hypothesis. This variable takes value around zero for  $\pi \pi \gamma$  events.

$\mathbf{E}_\pi^*(e)$  energy of the particle, identified as electrons by Time of Flight algorithm, calculated in  $K_S$  rest frame under pion mass hypothesis. In case of  $K_S \rightarrow \pi \pi$  decay energies of both outgoing particles in this selected frame will be equal to the half of the kaon energy ( $\sim 250$  MeV).

$\mathbf{M}^2(e) = (E_K - E(\pi) - p_{miss}(\pi, e))^2 - p^2(e)$   
 variable calculated only for particles identified as electrons and under assumption that massless particle occurs during the decay.

$$d_{PCA} = d_{PCA}(1) - d_{PCA}(2)$$

where  $d_{PCA}(1)$  ( $d_{PCA}(2)$ ) is the smallest distance between the Interaction Point and positive (negative) charged particle, calculated in the transverse plane. Value of  $d_{PCA}$  tests the quality of reconstructed vertex and due to that is sensitive to events in which pion decay into muon before entering the drift chamber.

In order to obtain the number of signal and background events in each category the normalization procedure is applied, based on previously described kinematic variables. Each event is assigned to one of the five regions in the  $\Delta E(\pi, e) - d_{PCA}$  plane illustrated in Figure 5.2. The choice of the regions and the assignment of the

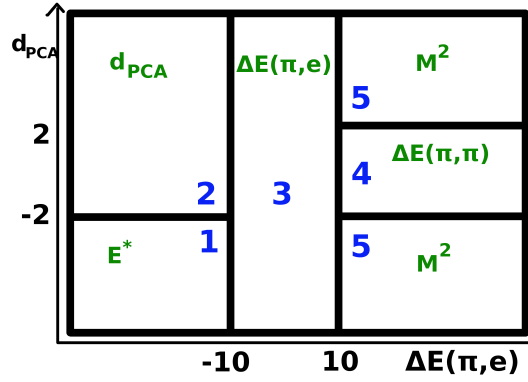


**Figure 5.2:** Definition of the fit regions in the  $\Delta E(\pi, e) - d_{PCA}$  plane. In each region the used variable is also specified.

fit variables ensure good separation between each component:

- in region 1 variable  $E_{\pi}^*(e)$  allows to recognize badly reconstructed  $\pi\pi$  events,
- in region 2 variable  $d_{PCA}$  is sensitive to pions that decay into muons before entering the drift chamber,
- in region 3 variable  $\Delta E(\pi, e)$  allows to separate signal events,
- in region 4 variable  $\Delta E(\pi\pi)$  enables selection of  $\pi\pi\gamma$  events,
- in region 5 variable  $M^2(e)$  is located around  $m_{\mu}^2$  mass for  $\pi \rightarrow \mu$  events.

Normalization is performed simultaneously over 5 regions by maximizing the follow-

Normalization category	Value of normalization parameter	
	$\pi^- e^+ \nu$	$\pi^+ e^- \bar{\nu}$
signal	0.8172(60)	0.8141(58)
$\pi\mu$	0.4920(47)	0.4029(52)
$\pi\pi$	1.4172(55)	1.3319(80)
$\pi\pi\gamma$	1.4171(11)	1.3349(17)
other	1.0629(13)	1.0012(81)
$\chi^2/\text{n.d.f.}$	1.62	0.96

**Table 5.1:** Summary of the obtained normalization parameters.

ing likelihood function:

$$\begin{aligned}
\mathcal{L} &= \prod_{r=1}^5 L^{(r)}, \\
\ln L^{(r)} &= \sum_{i=1}^{n(r)} \left[ d_i^{(r)} \ln f_i^{(r)} - f_i^{(r)} + \sum_{k=1}^m a_{ki}^{(r)} \ln A_{ki}^{(r)} - A_{ki}^{(r)} \right], \\
f_i^{(r)} &= \sum_{k=1}^m p_k A_{ki}^{(r)},
\end{aligned} \tag{5.1}$$

where the index  $r$  runs over 5 regions,  $i$  iterates bin of the variable chosen in the  $r^{\text{th}}$  region,  $n(r)$  denotes number of bins in  $r^{\text{th}}$  region,  $d_i^{(r)}$  is a number of data events that fall into bin  $i$  in  $r^{\text{th}}$  region.  $a_{ki}^{(r)}$  and  $A_{ki}^{(r)}$  are simulated numbers of events from  $k^{\text{th}}$  background component in  $i^{\text{th}}$  bin in case of finite and infinite statistics, respectively. The free parameters are the signal and background normalizations ( $p_k$ ). The details of used log-likelihood function ( $L^{(r)}$ ) are presented in [34] (subsection 7.7) and takes into account the finite statistics, as explained in [35]. In order to obtain a chi-square distributed variable the log-likelihood is normalized as explained in [36].

Obtained histograms and normalization parameters in each category are presented in Figure 5.3 and 5.4 and Table 5.1, respectively. Table 5.2 contains the number of events in each normalization subsample. It is necessary to remember that: events with initial or final state radiation [37], which are indistinguishable from "pure"  $K_S \rightarrow \pi e \nu$  decays, are assigned to semileptonic category,

Normalization category	Number of events obtained from normalization procedure	
	$\pi^-e^+\nu$	$\pi^+e^-\bar{\nu}$
signal	38157(280)	39662(282)
$\pi\mu$	22452(215)	15426(201)
$\pi\pi$	3224(10)	2879(29)
$\pi\pi\gamma$	2314(40)	1297(10)
other	1980(10)	1809(12)

**Table 5.2:** Final number of events obtained in each category.

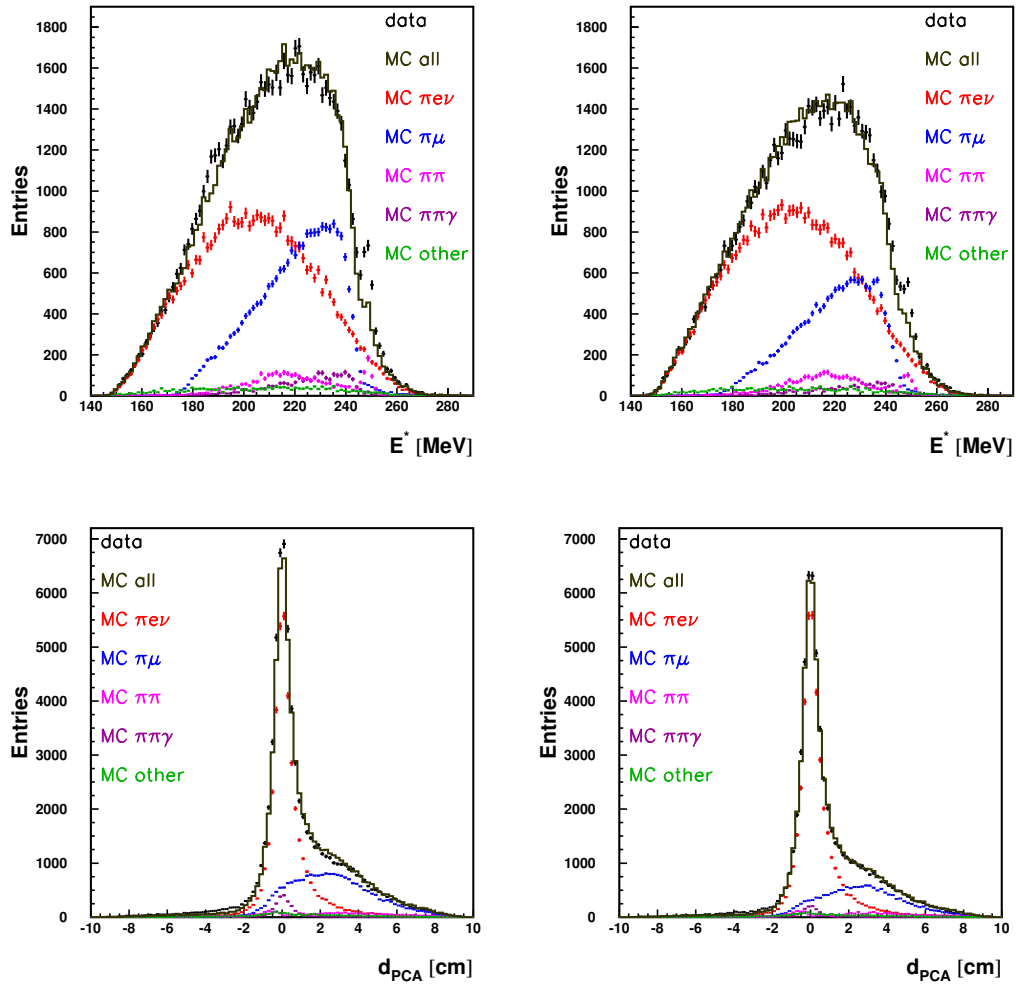


**Figure 5.3:** Data (points) and MC simulations (solid line) of  $E_{\pi^*}(e)$  (top row),  $d_{PCA}$  (bottom row) variables for charge  $\pi^-e^+\nu$  (left column) and  $\pi^+e^-\bar{\nu}$  (right column) after normalization procedure described in the text. Meaning of simulated histograms is described in the legends.

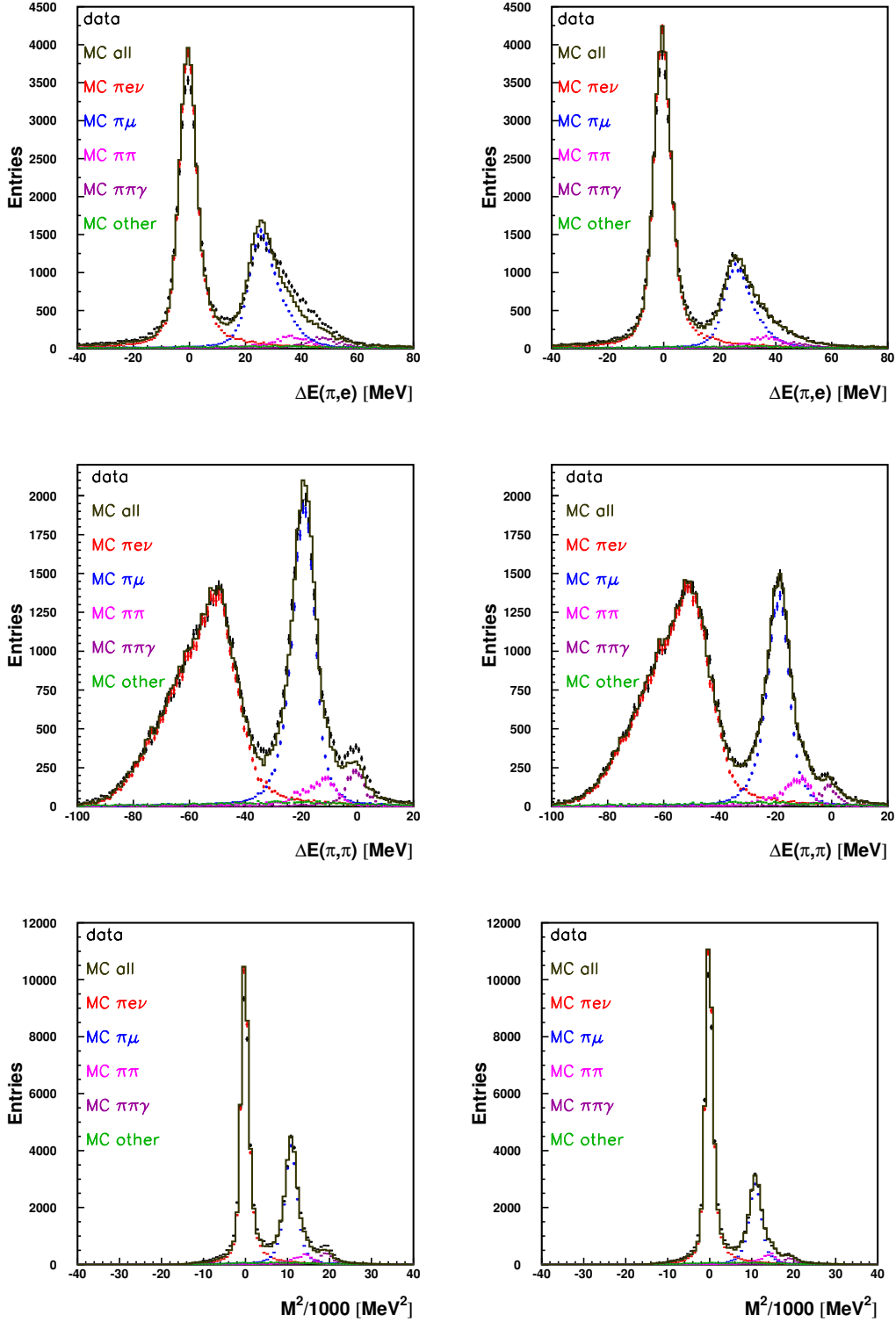


**Figure 5.4:** Data (points) and MC simulations (solid line) of  $\Delta E(\pi, e)$  (top row),  $\Delta E(\pi, \pi)$  (middle row) and  $M^2$  (bottom row) variables for charge  $\pi^- e^+ \nu$  (left column) and  $\pi^+ e^- \bar{\nu}$  (right column) after normalization procedure described in the text. Meaning of simulated histograms is described in the legends.

## 5.2 Estimation of the number of $K_S \rightarrow \pi^\mp e^\pm \nu(\bar{\nu})$ events

Total number  $N_{TOTAL}^\pm$  of the  $K_S \rightarrow \pi^\mp e^\pm \nu(\bar{\nu})$  events is given by the following expression:

$$N_{TOTAL}^\pm = \frac{n^\pm}{\epsilon_{TOTAL}^\pm} \quad (5.2)$$

where  $n^\pm$  is the number of the events selected for final states  $\pi^\mp e^\pm \nu(\bar{\nu})$  and  $\epsilon_{TOTAL}^\pm$  represents the probability to satisfy all of selection criteria and can be represent as:

$$\epsilon_{TOTAL}^\pm = \epsilon_{TRG} \cdot \epsilon_{FILFO} \cdot \epsilon_{stream} \cdot \epsilon_{crash} \cdot \epsilon_{DC} \cdot \epsilon_{TCA} \cdot \epsilon_{TOF} \cdot \epsilon_{CIRCLE} \quad (5.3)$$

with following efficiencies:

- $\epsilon_{TRG}$  - both kaons produced from  $\phi$  meson decay enters the acceptance of the detector and satisfy the trigger conditions [38, 39],
- $\epsilon_{FILFO}$  - probability to satisfy FILtro di FOndo (background filter) which identifies background events at a first stage of the data reconstruction only information from drift chamber only [40, 41].
- $\epsilon_{stream}$  - efficiency that  $\phi \rightarrow K_S K_L$  decay is classified in the neutral kaon stream [42, 43],
- $\epsilon_{crash}$  - probability to identify  $K_L$  interaction in calorimeter,
- $\epsilon_{DC}$  - probability to identify two tracks corresponding to oppositely charged particles that form a vertex near Interaction Point,
- $\epsilon_{TCA}$  - probability to associate both tracks to calorimeter clusters,
- $\epsilon_{TOF}$  - probability to satisfy Time of Flight identification,
- $\epsilon_{CIRCLE}$  - probability to satisfy „circle cut”,

Based on the assumption that the kaon final state is independent of  $\epsilon_{TRG}$ ,  $\epsilon_{FILFO}$ ,  $\epsilon_{stream}$  and  $\epsilon_{crash}$ , they will cancels out in the ratio of total efficiencies. Therefore, for the further estimation of charge asymmetry only number of events  $N^\pm$  after requirement of  $K_L(crash)$  can be taken into account:

$$N^\pm = \frac{n^\pm}{\epsilon_{tot}^\pm}, \quad (5.4)$$

where

$$\epsilon_{tot}^\pm = \epsilon_{DC} \cdot \epsilon_{TCA} \cdot \epsilon_{TOF} \cdot \epsilon_{CIRCLE}. \quad (5.5)$$

Summary of estimated efficiencies is shown in Table 5.3.

Efficiency	$K_S \rightarrow \pi^- e^+ \nu$	$K_S \rightarrow \pi^+ e^- \bar{\nu}$	$K_S \rightarrow \pi^+ \pi^-$
$\epsilon_{DC}$	0.7360(10)	0.7373(10)	0.0656(13)
$\epsilon_{TCA}$	0.4799(14)	0.4755(14)	0.6192(10)
$\epsilon_{TOF}$	0.8685(13)	0.8883(13)	0.0732(66)
$\epsilon_{CIRCLE}$	0.8757(14)	0.8975(13)	0.0816(26)
$\epsilon_{tot}$	0.2622(10)	0.2734(11)	$2.4237(79) \cdot 10^{-4}$

**Table 5.3:** Efficiency summary. For details see Chapter 4.

On the other hand obtained values  $N_{TOTAL}^\pm$  and  $N^\pm$  can be expressed as:

$$\begin{aligned}
N_{TOTAL}^\pm &= \mathcal{L} \cdot \sigma_\phi \cdot BR(\phi \rightarrow K_L K_S) \cdot BR(K_S \rightarrow \pi^\mp e^\pm \nu(\bar{\nu})) \\
N^\pm &= \mathcal{L} \cdot \sigma_\phi \cdot BR(\phi \rightarrow K_L K_S) \cdot BR(K_S \rightarrow \pi^\mp e^\pm \nu(\bar{\nu})) \cdot \epsilon \\
\epsilon &= \epsilon_{TRG} \cdot \epsilon_{FILFO} \cdot \epsilon_{stream} \cdot \epsilon_{crash}
\end{aligned} \tag{5.6}$$

where  $\mathcal{L}$  denotes integrated luminosity,  $\sigma_\phi$  is a cross section of  $\phi$  meson production,  $BR(\phi \rightarrow K_L K_S)$  and  $BR(K_S \rightarrow \pi^\mp e^\pm \nu(\bar{\nu}))$  are branching ratios of  $\phi \rightarrow K_L K_S$  and  $K_S$  semileptonic decays, respectively.

### 5.3 Charge asymmetry

The charge asymmetry is given by:

$$A_S = \frac{\Gamma(K_S \rightarrow \pi^- e^+ \nu) - \Gamma(K_S \rightarrow \pi^+ e^- \bar{\nu})}{\Gamma(K_S \rightarrow \pi^- e^+ \nu) + \Gamma(K_S \rightarrow \pi^+ e^- \bar{\nu})} = \frac{n^+/\epsilon_{tot}^+ - n^-/\epsilon_{tot}^-}{n^+/\epsilon_{tot}^+ + n^-/\epsilon_{tot}^-}. \tag{5.7}$$

Using the  $1.7\text{fb}^{-1}$  total luminosity data sample collected at KLOE in 2004-2005 and values provided in previous sections, the following result is obtained:

$$A_S = (1.5 \pm 5.8_{stat}) \cdot 10^{-3}, \tag{5.8}$$

which, compared to  $A_L = (3.322 \pm 0.058_{stat} \pm 0.047_{syst}) \cdot 10^{-3}$  [7], does not indicate the violation of  $\mathcal{CPT}$  symmetry. The systematic uncertainty was not determined so far, but we expect to obtain systematical error as 25% of total uncertainty as in previous KLOE measurement of  $K_S$  charge asymmetry, which was equal  $A_S = (1.5 \pm 9.6_{stat} \pm 2.9_{syst}) \cdot 10^{-3}$  [8].

## Chapter 6

# Conclusions

The aim of this work is to test  $\mathcal{CPT}$  violation in neutral kaon systems via the comparison between charge asymmetries for  $K_S$  and  $K_L$  semileptonic decays. The  $A_L$  was measured with a high precision  $A_L = (3.322 \pm 0.058_{\text{stat}} \pm 0.047_{\text{syst}}) \cdot 10^{-3}$  by KTeV collaboration [7]. The most precise measurement of  $A_S$  was performed by KLOE collaboration,  $A_S = (1.5 \pm 9.6_{\text{stat}} \pm 2.9_{\text{syst}}) \cdot 10^{-3}$  [8], however the accuracy of  $A_S$  determination is more than two orders of magnitude worse than this of  $A_L$  determination and the main contribution gives the statistical uncertainty which is three times larger than systematical. Therefore, in this work a new measurement of  $A_S$  based on around four times bigger data sample collected by means of the KLOE detector in 2004 and 2005, is presented.

The analysis exploits a tagging technique of search for  $K_L$  mesons that reach the calorimeter, which allows to identify  $K_S$  decay on the other side of  $\phi$  meson decay and, due to this, around  $0.5 \times 10^{12}$  of  $K_S$  mesons were tagged. In next step the  $K_S \rightarrow \pi e \nu$  decay is selected based on its kinematics. The Time of Flight algorithm, which allows to select interesting events with high precision, is also used. The number of events due to the signal and each background categories are evaluated through the normalization procedure. Altogether around  $78 \times 10^3$  of  $K_S \rightarrow \pi e \nu$  decays was reconstructed, which allows to obtain the following value for the  $K_S$  semileptonic asymmetry:

$$A_S = (1.5 \pm 5.8_{\text{stat}}) \cdot 10^{-3}. \quad (6.1)$$

The achieved statistical uncertainty is about two times better with respect to the previous measurement [8]. The obtained value of  $A_S$  is equal within error bars to the  $A_L$ , which is consistent with no violation of  $\mathcal{CPT}$  symmetry. In the future a new detector KLOE-2 shall improve the further experimental accuracy of the determination of  $K_S$  semileptonic decays and associated quantities [44]



## *Acknowledgements*

I would like to express my deepest gratitude to dr Eryk Czerwiński and prof. Paweł Moskal, my research supervisors, for the immeasurable amount of support and guidance they have provided throughout this study.

I would also like to extend my appreciation to prof. Antonio Di Domenico, dr Erika de Lucia and dr Antonio De Santis for their constructive comments and warm encouragement during our meetings.

I would like to offer my special thanks to prof. Wojciech Wiślicki, dr. Michał Silarski and dr Wojciech Krzemień for their suggestions and remarks during our group meetings.

Moreover, I would like to thank prof. Bogusław Kamys for giving me opportunity to work in the Nuclear Physics Division of the Jagiellonian University.

I also thank to my colleagues mgr Aleksander Gajos, mgr Izabela Pytko, Krzysztof Kacprzak and dr Jarosław Zdebik for a nice atmosphere during the work.

And at the end, I wish to thank my family for giving me the opportunity to follow my dreams. Furthermore, I would like to thank my partner, just for being close to me, and his family for warm welcome at family circle.

This work was supported by the Foundation for Polish Science through the project HOMING PLUS BIS/2011-4/3 and the MPD programme; the European Commission under the 7th Framework Programme through the 'Research Infrastructures' action of the 'Capacities' Programme, Call: fp7-infrastructures-2008-1, Grant Agreement No. 227431 and by the Polish National Science Centre through the Grant No. 2011/01/D/ST2/00748.



# Bibliography

- [1] A. E. Noether, “Invariante Variationsprobleme”, *Nachr. d. onig. Gessellsch. d. Wiss. zu ottingen, Math-phys. Klasse.*, (1918), pp. 235–257.
- [2] N. Cabibbo, “Unitary Symmetry and Leptonic Decays”, *Phys. Rev. Lett.* 10 (1963), pp. 531–533.
- [3] Z. Maki, M. Nakagawa, S. Sakata, “Remarks on the Unified Model of Elementary Particles”, *Prog. of Theor. Phys.* 28.5 (1962), pp. 870–880.
- [4] V. A. Kostelecky, N. Russell, “Data Tables for Lorentz and CPT Violation”, *Rev. Mod. Phys.* 83 (2011), pp. 11–31, arXiv: [0801.0287 \[hep-ph\]](#).
- [5] O. W. Greenberg, “CPT violation implies violation of Lorentz invariance”, *Phys. Rev. Lett.* 89 (2002), p. 231602, arXiv: [hep-ph/0201258 \[hep-ph\]](#).
- [6] L. Maiani, G. Pancheri, N. Paver, *The Second DAΦNE Physics Handbook*, Istituto nazionale di fisica nucleare. Laboratori nazionali di Frascati, 1995.
- [7] KTeV Collaboration, “A measurement of the  $K_L$  charge asymmetry”, *Phys. Rev. Lett.* 88 (2002).
- [8] KLOE-2 Collaboration, “Study of the branching ratio and charge asymmetry for the decay  $K_S \rightarrow \pi e \nu$  with the KLOE detector”, *Phys. Lett. B.* 636 (2006), pp. 173–182.
- [9] KLOE-2 collaboration, “Observation of the rare  $\eta \rightarrow e^+ e^- e^+ e^-$  decay with the KLOE experiment”, *Phys. Lett. B.* 702 (2011), pp. 324–328, arXiv: [1105.6067 \[hep-ex\]](#).
- [10] KLOE Collaboration, “Measurement of the branching ratio and search for a CP violating asymmetry in the  $\eta \rightarrow \pi^+ \pi^- e^+ e^- (\gamma)$  decay at KLOE”, *Phys. Lett. B.* 675 (2009), pp. 283–288, arXiv: [0812.4830 \[hep-ex\]](#).
- [11] KLOE-2 Collaboration, “Limit on light gauge boson production in  $e^+ e^- \rightarrow \mu^+ \mu^- \gamma$  interactions with the KLOE experiment” (2014), arXiv: [1404.7772 \[hep-ex\]](#).
- [12] C. Butler, G. Rochester, “Evidence for the existence of new unstable elementary particles”, *Nature* 160 (1947), pp. 855–857.
- [13] M. Gell-Mann, “Isotopic spin and new unstable particles”, *Phys. Rev.* 92 (1953), pp. 833–834.
- [14] K. Nishijima, “Some remarks on the even-odd rule”, *Prog. of Theor. Phys.* 12 (1954), pp. 107–108.

- [15] F. Halzen, A. D. Martin, *Quarks and leptons*, John Wiley and Sons, 1984.
- [16] M. Gell-Mann, A. Pais, “Behavior of neutral particles under charge conjugation”, *Phys. Rev.* 97.5 (1955), pp. 1387–1389.
- [17] J. Christenson, J. Cronin, V. Fitch, R. Turlay, “Evidence for the  $2\pi$  Decay of the  $K_2^0$  meson”, *Phys. Rev. Lett.* 13 (1964), pp. 138–140.
- [18] Particle Data Group Collaboration, “Review of Particle Physics (RPP)”, *Phys. Rev.* D86.010001 (2012).
- [19] C. Gatti, “Measurement of the branching fraction for the decay  $K_S \rightarrow \pi^\pm e^\mp \nu(\bar{\nu})$  with the KLOE detector”, PhD thesis, Univerita degli Studi di Pisa, 2002.
- [20] F. Archilli, “ $K_S$  decay studies with the KLOE experiment: upper limit for the transition  $K_S \rightarrow e^+e^-$  and charge asymmetry for the semileptonic decay  $K_S \rightarrow \pi e \nu$ ”, PhD thesis, Universita Degli Studi di Roma Tor Vergata, 2003.
- [21] CPLEAR Colaboration, “A determination of the CPT violation parameter  $Re\delta$  from the semileptonic decay of strangeness-tagged neutral kaons”, *Phys. Lett.* B.444 (1998), pp. 52–60.
- [22] KLOE Collaboration, “The KLOE detector: technical proposal” (1993).
- [23] KLOE Collaboration, “Precision Kaon and Hadron Physics with KLOE”, *Riv. Nuovo Cim.* 31 (2008), pp. 531–623, eprint: [0811.1929](https://arxiv.org/abs/0811.1929).
- [24] G. Morello et al., “The cylindrical GEM detector for the KLOE-2 Inner Tracker”, *JINST* 9 (2013).
- [25] A. Balla et al., “QCALT: A tile calorimeter for KLOE-2 upgrade”, *Nucl. Instrum. Meth.* A718 (2013), pp. 95–96.
- [26] M. Cordelli et al., “CCALT: A Crystal CALorimeter with Timing for the KLOE-2 upgrade”, *Nucl. Instrum. Meth.* A718 (2013), pp. 81–82.
- [27] G. Vignola, M. Bassetti, M. E. Biagini, C. Biscari, R. Boni, “DAPHNE, the first Phi-factory”, *Conf. Proc.* C960610 (1996), pp. 22–26.
- [28] *FINUDA experiment website*, [www.lnf.infn.it/esperimenti/finuda/finuda.html](http://www.lnf.infn.it/esperimenti/finuda/finuda.html), Accessed 2014-03-20.
- [29] S. Bianco, “DEAR, FINUDA, KLOE: Kaonic atoms, hypernuclei and CP violation at the DAPHNE phi factory” (1997), arXiv: [hep-ex/9712026](https://arxiv.org/abs/hep-ex/9712026) [hep-ex].
- [30] *SIDDHARTA experiment website*, [www.lnf.infn.it/esperimenti/siddharta/](http://www.lnf.infn.it/esperimenti/siddharta/), Accessed 2014-03-20.
- [31] KLOE Collaboration, “A new limit on the CP violating decay  $K_S \rightarrow 3\pi^0$  with the KLOE experiment”, *Phys. Lett.* B723 (2013), pp. 54–60, arXiv: [1301.7623](https://arxiv.org/abs/1301.7623) [hep-ex].
- [32] M. Paterno, “Calculating efficiencies and their uncertainties” (2004).
- [33] C. Gatti, T. Spadaro, *Measurement of the branching fraction and the charge asymmetry for the decay  $K_S \rightarrow \pi e \nu$* , KLOE Note 208, 2006.
- [34] CERN Information Technology Division, *HBOOK Statistical Analysis and Histogramming*, Reference Manual, 1998.
- [35] C. Beeston R. Barlow, “Fitting using finite Monte Carlo samples”, *Comput. Phys. Commun.* 77 (1993), pp. 219–228.

- 
- [36] S. Barker, R. D. Cousin, “Clarification of the use of chi-square and likelihood function in fits to histogram”, *Nucl. Inst. Meth.* A.221 (1983).
  - [37] C. Gatti, *MC generators for radiative kaon decays*, KLOE Note 194, 2004.
  - [38] KLOE Collaboration, *The KLOE trigger system*, LNF-96/043, 1996.
  - [39] B. Sciascia, “Studies of charged kaon decays with the KLOE experiment”, PhD thesis, University La Sapienza (Rome), 2000.
  - [40] G. Finocchiaro, A. Menicucci, *Cosmic ray rejection in KLOE*, KLOE Memo 203, 1999.
  - [41] M. Moulson, S. Muller, *FILFO revisited: A new look at the offline reconstruction filter and event classification*, KLOE Memo 288, 2004.
  - [42] C. Bloise, M. Incagli, *The Event Classification module and the ECLO, ECLS banks*, KLOE Memo 175, 1999.
  - [43] C. Bloise, M. Incagli, *The Event Classification procedures*, KLOE Memo 225, 2000.
  - [44] KLOE-2 Collaboration, “Physics with the KLOE-2 experiment at the upgraded DAΦNE”, *Eur. Phys. J.* C68 (2010), pp. 619–681, arXiv: [1003.3868 \[hep-ex\]](#).